ACS OMEGA

http://pubs.acs.org/journal/acsodf

Article

Experimental Study of the Growth Kinetics of Natural Gas Hydrates in an Oil−Water Emulsion System

Xiaofang Lv,* Jie Zhang, Yi Zhao, Yang Liu,* Jiawen Xu, Qianli Ma, Shangfei Song, and Shidong Zhou

Cite This: *ACS Omega* 2022, 7, 599−616

Read Online

ACCESS | Metrics & More | Article Recommendations

ABSTRACT: In order to explore the growth kinetics characteristics of NGH (natural gas hydrate) in an oil and gas mixed transportation pipeline and ensure the safe transportation of the pipeline, with the high-pressure hydrate experimental loop, an experimental study on the growth characteristics of NGH in an oil−water emulsion system was carried out, and the effects of pressure, flow rate, and water cut on the hydrate induction time, gas consumption, consumption rate, and hydrate volume fraction were explored, and important experimental rules were obtained. The experiment was divided into three stages: in the rapid formation stage of the hydrate, the temperature and gas consumption rose sharply, and the pressure dropped suddenly. The induction time decreased with the increase of pressure, flow rate, and water cut. The induction time of 6 MPa was 86.13 min, which was shortened by 39.68% compared with the induction time of 142.8 min of 5 MPa. The induction time of 1500 kg/h was 88.27 min, which was shorter by 13.91% than that 102.53 min of 550 kg/h. The induction time of 20% water cut was 58.53 min, which was shorter by 13.99% than that 68.4 min of 15% water cut. The gas consumption and hydrate volume fraction were both increased with the increase of pressure and water cut and decreased with the increase in the flow rate. In the whole process of the formation of NGH, the consumption rate first increased and then decreased. The pressure-drop and apparent viscosity increased with the increase of hydrate volume fraction in a certain range. The sensitivity analysis of hydrate induction time based on the standard regression coefficient method showed that the initial pressure played a major role, followed by the flow rate and the water cut. Based on the sensitivity analysis of hydrate volume fraction by the gray correlation method, it was found that the hydrate volume fraction had the closest relationship with the initial pressure, followed by the flow rate and the water cut. Finally, the empirical formulas of induction time and hydrate volume fraction in an oil−water emulsion system were established.

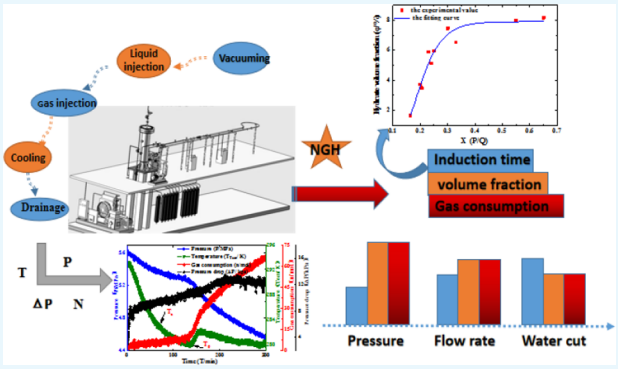

1. INTRODUCTION

With the development of oil and gas resources gradually moving from the land to the ocean, the study on the growth kinetic characteristics of hydrates under the oil and gas mixed transportation system with high pressure and low temperature had become a hot issue in the industry.[1,2]The high-pressure and low-temperature environment in deep sea provided convenient conditions for the formation of natural gas hydrate (NGH), but at the same time, it also brought great challenges for the safe transportation of NGH.[3−5] In view of this, the application of risk prevention and control technology was born. This new risk control technology allowed the hydrate to be transported in the form of slurry in the pipeline, which had the advantages of low-cost and environmentally friendly. It could alleviate the disadvantages of low natural gas transportation efficiency in the traditional pipeline transportation process and had gradually become the focus of the current research.[6−8] The studies of hydrate growth kinetics were the basis of risk control technology. However, there was still a lack of comprehensive understanding of the hydrate formation mechanism and growth kinetics. This would directly affect the quantitative calculation and risk assessment of gas hydrate transport by pipelines. In the study of hydrate growth kinetics, the induction time, gas consumption, and hydrate volume fraction were the key parameters that affect the safe and stable transportation of NGH. These key parameters would be affected by pressure, flow rate, water cut, and so forth. Therefore, the safe transportation process of deep-sea hydrate slurry must deeply explore the basic theoretical issues of the formation mechanism and hydrate growth dynamics, so as to

Received: September 15, 2021
Accepted: December 9, 2021
Published: December 21, 2021

© 2021 The Authors. Published by American Chemical Society

https://doi.org/10.1021/acsomega.1c05127
ACS Omega 2022, 7, 599−616

obtain not only the key parameters to ensure the safe transportation of slurry in practical mixed transportation pipelines but also the general laws to improve slurry transportation efficiency.[9−11]

At present, the research results of hydrate growth kinetics in the oil−water emulsion system were as follows: in terms of microscopic experiments, Sun[12] and Chen used laser scattering technology to describe that the particle diameter during hydrate formation increased rapidly from the initial reaction stage to the maximum and finally tended to be stable. When the flow rate of the system was increased, the average diameter decreased, and the particle distribution curve moved to the left. Song[13] et al. captured the micromorphology and microflow behavior of hydrate particles with high-speed cameras and found that in the hydrate slurry, the proportion of small hydrate particles gradually decreased, while that of large hydrate particles gradually increased. In addition, the average particle size of hydrate particles gradually increased during the flow process and eventually tended to be stable. The particle size distribution of hydrate in the flow field accorded with normal distribution. Lv[14,15] found that there were two peaks in the size distribution of hydrate particles based on the FBRM. When the hydrate started to form, the particles aggregated to reach the first peak, and then, under the effect of shear force, the aggregation was dispersed into small particles, the particle size gradually decreased, the fluid viscosity increased, the flow rate decreased, the particles gradually gathered and deposited, and finally blocked the pipeline to reach the second peak. The influence of the dosage of antiagglomerant and water cut on the particle size was studied. The results showed that the particle size decreased with the increase of the dose of antiagglomerant and that the particle size increased with the increase of water cut. Under high shear force, the smaller the diameter was, the better the slurry transportation was in a certain pipe length. This indicated that the microscopic characteristics of hydrate particles would be affected by factors such as flow rate, dosage, and water cut and then showed different characteristics, affecting the safe operation of mixed transport pipelines.[16] In addition, the microscopic characteristics of hydrate particles also affected the macroscopic parameters of the slurry, and the interaction between microscopic characteristics and macroscopic parameters resulted in the complexity and variability of the slurry.

Balakin[17] et al. found that the slurry viscosity depended on the size of hydrate particles and the adhesion between particles. Cao[18] et al. established a rheological prediction model to simulate the variation of slurry viscosity with hydrate particle size and verified the feasibility of the model in combination with experimental data; it was found that when the particle diameter increased from 142 to 293 μm, the flow stability of stratified flow increased. In slug flow, the viscosity and density of the hydrate slurry would increase with the collision and coalescence of particles, thus weakening or inhibiting the flow of the hydrate slurry. On the contrary, flow patterns could also affect the microscopic characteristics of hydrate particles. Ding[19] et al. discussed the influence of flow patterns on hydrate phase transformation and microscopic behavior and established a comprehensive model for the agglomeration and deposition of NGH under different flow patterns. Liu[20] et al. studied the influence of particle agglomeration on the flow characteristics of the gas hydrate slurry and found that the agglomeration of hydrate particles would increase the pressure drop of the hydrate slurry, while the pressure drop decreased slightly in the process of particle deposition. Sun[21] used FLUENT to simulate the flow of hydrate slurry in a horizontal pipe and found that with the gradual increase of hydrate particle size, the pressure-drop of the hydrate slurry also gradually increased.

To sum up, the microscopic characteristics of hydrate particles were the essential factors affecting the hydrate growth kinetics. At present, the research on hydrate growth dynamics mainly focused on hydrate growth and nucleation. However, the aggregation characteristics of hydrate particles were the main cause of pipeline blockage, and corresponding measures should be taken to prevent the accumulation of hydrate particles.

In terms of macro experiments, Shi[22] et al. explored the variation of induction time of gas hydrate formation with system pressure and flow rate and found that high pressure and large flow rate would shorten the induction time, but higher pressure would also aggravate the risk of pipe plugging while accelerating the rate of hydrate generation.[23]an[24] et al. analyzed and compared the inhibition effect of combined antiagglomerant and the single antiagglomerant on hydrate formation in an oil−water system. The results showed that the use of combined antiagglomerant before hydrate formation could effectively inhibit the nucleation and growth of hydrate particles and prolong the hydrate induction period. However, in the process of hydrate formation, the addition of combined antiagglomerant would cause the coalescence of hydrate particles and eventually led to pipeline blockage. The above research results showed that in the actual pipeline operation, the flow rate and pressure should not be too high. Adding a dose of antiagglomerant, adding time of antiagglomerant, and use of combined antiagglomerant were important factors affecting the safe operation of pipelines.[25,26]

Chen[27] et al. explored the influence of water cut, the amount of Span20, and the degree of supercooling on the induction period of methane hydrate with the high-pressure reactor and found that the degree of undercooling was the main factor affecting the induction time. When the degree of supercooling was greater than 4 K, the average formation time of methane hydrate was less than 200 min. However, considering that the flow system was more in line with the actual flow of NGH, the experimental data of the loop were more convincing. Therefore, Sun[28] et al. measured the induction time in (R12 + water) and (CH_4 + THF + water) systems by a U-bend tube and found that the induction time was exponentially related to the driving force, and the flow rate also had a significant effect on the hydrate nucleation. In view of this, a new induction time model shown as eq 1 combining the driving force and the flow rate was proposed, which was in good agreement with the experimental data. However, this model was relatively simple and involved fewer parameters. The system used was limited.

$$T_{\text{induction time}} = K_{\text{Sun}} \left\{ \frac{f_g^v}{f_{eg}} \sqrt{Q/Q_0} - 1 \right\}^{-m\text{Sun}} \quad (1)$$

Chen[29] et al. considered that the presence of wax in the actual mixed pipeline would seriously affect the slurry flow safety, so the induction time model of NGH shown as eq 2 in the waxy water-in-oil emulsion system was established based on the model proposed by Kashchiev[30] and Firoozabadi. However, this model was only applicable to the static reaction

https://doi.org/10.1021/acsomega.1c05127
ACS Omega 2022, 7, 599−616

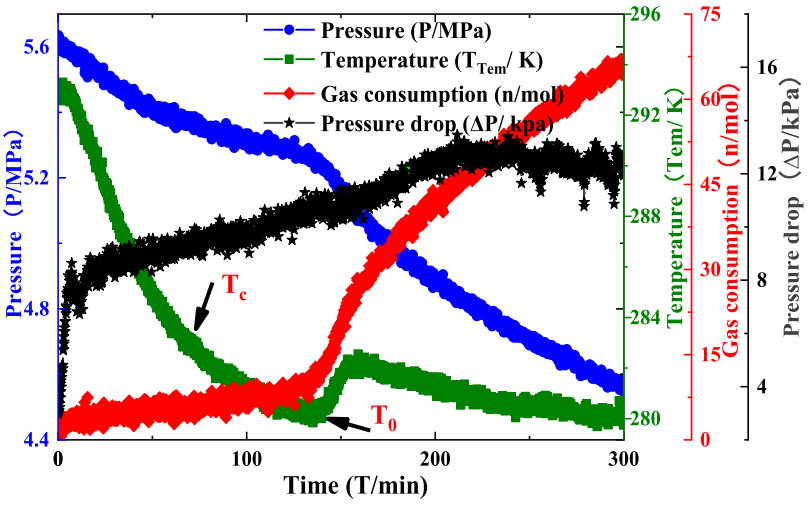

Figure 1. Variation of gas consumption, temperature, pressure, and pressure drop with time.

system, and its application to the flow system remained to be studied.

$$T_{(\text{induction}-\text{time}-\text{wax})} = (1 + K_F C_{\text{wax}}^{1/n_{\text{chen}}} K_{\text{chen}} \left[S[(S-1)^3]^{-1/4} \exp\left(\frac{B_{\text{chen}}}{4 \ln^2 s}\right)\right] \quad (2)$$

In addition to wax, many other impurities in the system also affected the induction time. Zi[31] et al. found that the presence of silica sand could greatly shorten the induction time of methane hydrate in the oil-in-water emulsion. Wang[32,33] et al. increased the sand particle size and found that the induction time was significantly shortened. However, Chen[34] et al. reached a completely different conclusion: at the gas−water interface, the presence of sand particles could prevent methane gas from entering the water, inhibit the nucleation of hydrate, and lead to the increase of induction time. Therefore, complex fluid composition and variable flow parameters aggravated the difficulty of hydrate induction time research. Therefore, future studies should focus on multifactor coupling analysis to provide a more theoretical basis for the actual mixed transportation pipeline.[35]

In addition to induction time, the pressure-drop, viscosity, and so forth were also affected by many factors. As an important parameter of slurry safe flow, pressure drop was affected by flow rate, water cut, initial pressure, hydrate volume fraction, and so on. Prah[36] and Yun studied the pressure drop characteristics of CO_2 hydrate in the flow loop and found that the pressure drop gradient increased with the increase of the average flow rate of hydrate. Basha[37] et al. conducted slurry flow experiments with different water cuts and found that when the water cut was 0−40%, the pressure drop decreased, and with the increase of water cut, the pressure-drop increased. In view of this, domestic and foreign scholars had established pressure drop prediction models under different systems. Chen[38] et al., taking into account the hydraulic action, particle collision effect caused by particle aggregation, and energy dissipation caused by hydrate−liquid friction, established a pressure drop prediction model under turbulent flow conditions, which could better describe the flow characteristics of the hydrate slurry. Zhang[39] established a prediction model of pressure drop during the deposition process by considering the porosity of the hydrate deposition layer and the hydrate deposition behavior of condensate near the cold wall, which provided a theoretical basis for the gas transport efficiency and safety of pipelines in seabed and cold regions.

There were many factors affecting slurry viscosity,[40] including system temperature, pressure, shear rate, flow rate, water cut, and so forth. Domestic and foreign scholars have carried out experiments on the viscosity of hydrate slurry in different systems such as TBAB,[41] TBAF,[42] TBPB,[43] THF, HCFC-141B,[44] and CO_2[45] with the help of experimental devices such as reactors, loop, or rheometers. Based on the power law, Herschel−Bulkley, and cross constitutive equations, some viscosity prediction models were proposed. Camargo and Palermo[46] proposed an effective theoretical medium viscosity model considering the agglomeration of hydrate particles, which had been widely recognized by hydrate researchers. Chen[47,48] et al. analyzed the viscosity of the hydrate slurry with the help of a U-shaped bend pipe and established the power law model and Herschel−Bulkley model. The results showed that the non-Newtonian property of the hydrate slurry became more obvious with the increase of hydrate volume fraction. Shi[49] et al. studied the viscosity of hydrate slurry in waxy and no-wax systems with the help of the rheological measurement system. Based on the effective theoretical medium viscosity model established by Camargo[46] and Palermo, particle number, particle Reynolds number, and particle Weber number were introduced to describe the effects of hydrate aggregation and fragmentation on its viscosity, and a semiempirical model of applicability was established.

Although the viscosity and pressure drop prediction models established at present had good applicability in a specific system, the results were not ideal when applied to other systems, and there were certain deviations. Therefore, in the following studies, the model should be optimized and explored from the aspects of comprehensive analysis of different systems, the property parameters of hydrate particles, and the coupling relationship between hydrate and multiphase flow in order to achieve a more accurate description of the actual slurry flow.

To sum up, in terms of macroscopic experiments, a large number of experimental studies on hydrate growth dynamics had been carried out by predecessors, and important theoretical results have been obtained, providing guidance

https://doi.org/10.1021/acsomega.1c05127
ACS Omega 2022, 7, 599−616

for hydrate formation prediction and hydrate risk control technology. However, there was still a lack of comprehensive understanding of the influence of key factors such as pressure, flow rate, and water cut on hydrate growth kinetics in the whole flow system. Induction time, gas consumption, and volume fraction were the most important parameters of hydrate growth kinetics, and the accuracy of their quantitative characterization needed to be improved. The influence degree of key factors on the parameters of hydrate growth kinetics was the key to further determine the prediction model, but the sensitivity analysis of the influence degree of key parameters in relevant experiments had not been carried out in detail. At present, the established prediction model was based on a static system, or involved few influence parameters, or only applied to specific system, so it was not able to describe the actual flow situation comprehensively. Based on this, the author carried out an experimental study on the growth kinetic characteristics of oil−water emulsion NGH with the help of a high-pressure hydrate experiment loop. Taking the initial pressure, initial flow rate, water cut, and other key factors that affect the hydrate growth kinetics into consideration, the growth kinetic parameters such as induction time, gas consumption, volume fraction, and so on were comprehensively analyzed to quantitatively characterize the growth kinetic characteristics of hydrate. Sensitivity analysis of induction time and hydrate volume fraction was conducted to determine the primary and secondary influencing factors, so as to improve the prediction accuracy of the quantitative characterization model. This paper could provide strong support for the application of new hydrate risk control technology.

2. RESULTS AND DISCUSSION

2.1. Analysis of Typical Experimental Phenomena.

The experiment was carried out under the water-bath temperature at 1 °C, the flow rate of 550 kg/h, and the pressure of 5 MPa. The results are shown in Figure 1. It could be seen from the figure that temperature, pressure, gas consumption, and pressure drop all changed with the running time. The variation trend was similar to the growth characteristics of NGH in the oil-in-water emulsion system described in the previous literature,[50−52] and the experimental process could be roughly divided into three stages.

The stage of induction period: the temperature dropped sharply because of the cooling of the cryogenic water bath, and the solubility of natural gas in the liquid phase gradually increased with the decrease of temperature, resulting in the gas dissolving and absorbing the surrounding heat, and the temperature dropping again, when reduced to the equilibrium temperature T_C, led the system into the induction period. Until the temperature was reduced to T_0. The induction period ended, the period of $T_C - T_0$ was called macroscopic induction time, when the system temperature reached the lowest point. The hydrate formation curve could be defined by the Chen−Guo[53] model and natural gas composition, as shown in Figure 2. The dissolution of natural gas in the liquid phase caused the pressure of the system to decrease uniformly. The change of gas consumption was not obvious and showed a trend of slow rise. The pressure drop fluctuated up and down in a small range, which might be caused by the magnetic circulating pump used in the experiment. It could be observed through the visible tube section that the fluidity in the tube was good at this time, and there was no hydrate generation.

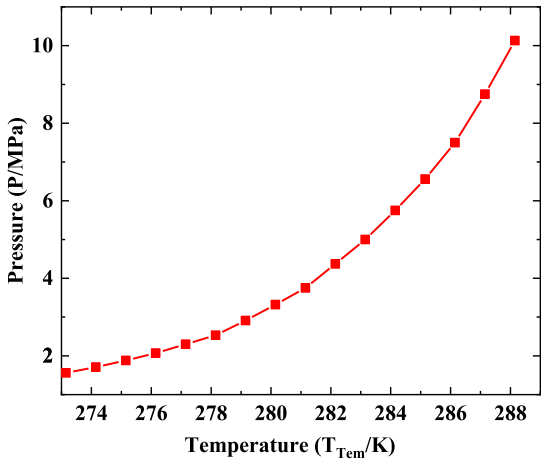

Figure 2. Hydrate formation curve.

The stage of hydrate massive formation: when the temperature dropped to T_0, the system reached the thermodynamic conditions for the formation of gas hydrate. At the end of the induction period, the hydrate began to form. Because the temperature of the water bath jacket was lower than the temperature of the system, it could be observed through the visible pipe section that the first hydrate forms on the wall surface. Due to the exothermic reaction of hydrate generation, the temperature of the system rose rapidly in a short time. The temperature of the loop temperature measuring point detected that the temperature rose from 279.99 to 281.87 K. Gas hydrate generation consumed a lot of natural gas, so the rate of pressure drop increased obviously. The gas consumption and the consumption rate increased obviously. The formation of hydrate increased the slurry viscosity, so the pressure drop increased in a fluctuating manner with a large range of changes. At this time, the fluctuation might be caused by the system vibration due to the collision and coalescence of hydrate particles. The hydrate on the wall slides down and flowed with the liquid phase under shear force between the pump and the fluid, and the flow state was good.

The stage of hydrate slurry stable flow: soon after the time T_0, the temperature began to drop again, mainly because the rate of hydrate formation decreased, and the heat released from hydrate formation was lower than that of water bath cooling. Because the amount of dissolving gas was reduced, the pressure dropped slowly. Gas consumption increased slowly, indicating that hydrate was still forming, but the consumption rate slowed down. When the pressure no longer dropped, the temperature reached the water bath temperature and remained stable, and the gas consumption reached the maximum, hydrate was no longer forming, and the slurry flowed steadily.

Through the above experimental data and phenomena, it could be obtained that the parameters of pressure, temperature, gas consumption, and pressure drop changed from the induction period to the steady flow of the slurry, which showed that the temperature dropped from the beginning to the sudden rise of hydrate formation and then to the slow decline. The pressure declined slowly at the beginning to a sharp drop when the hydrate was formed and then to a slow drop. The gas consumption increased slowly at the beginning to a sharp rise when hydrate was formed and then remained stable. The pressure drop changed from not obvious at the beginning to fluctuate increased at the time of hydrate formation and then

https://doi.org/10.1021/acsomega.1c05127
ACS Omega 2022, 7, 599−616

to be stable. These experimental results had a good guide to the study of the growth characteristics of NGH.

2.2. Influence of Different Pressures on the Hydrate Growth Kinetics. *2.2.1. Influence of Different Pressures on the Hydrate Induction Period.* By changing the initial pressure of the system (4.1, 5, and 6 MPa), the experiment studied the influence of the initial pressure in the pipeline flow system on the hydrate induction period. Due to the randomness of the hydrate induction time, 3−5 repeated measurement experiments were carried out under the same condition and the induction time was recorded each time, as shown in Figure 3. It showed that the experiment had good repeatability and the data of induction time were basically accurate.

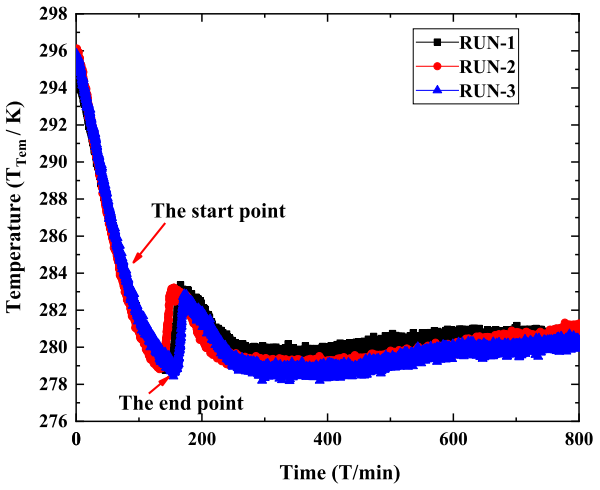

Figure 3. Natural gas induction time during three reproduced formation experiments in the flow-loop.

The experimental parameters are shown in Table 1. According to Table 1, under the temperature of 270.15 K and flow rate of 1200 kg/h, the induction times corresponding to different initial pressures were 120.50, 90.27, and 84.43 min, respectively. Under the temperature of 274.15 K and flow rate of 1500 kg/h, the induction times corresponding to different initial pressures were 208.67, 123.80, and 75.43 min, respectively. When the initial pressure increased from 4.1 to 5 MPa, the induction time was shortened by 25.08 and 40.67%, and when the initial pressure increased from 5 to 6 MPa, the induction time was shortened by 6.46 and 39.07%, respectively. Therefore, the induction time of NGH decreased with the increase of initial pressure. This phenomenon could be explained as follows: according to the hydrate growth kinetics theory, the increase of initial pressure led to the increase of supersaturation of the system, and then, the driving force of hydrate crystallization became larger and the nucleation and crystallization rate accelerated, so the hydrate induction period was shorter. According to the experiment of Maeda,[54] this conclusion was also applicable to the static reactor system. Factors such as temperature and degree of undercooling and supersaturated had important effects on the hydrate induction period as well as pressure, which could be mainly attributed to the change of driving force of hydrate nucleation. Therefore, with the decrease of temperature and the increase of subcooling degree and supersaturation degree, the driving force of hydrate crystallization nucleation increased and the hydrate induction period shortened. In an actual pipeline, pressure, subcooling, and supersaturation driving forces should not be too large and the temperature should not be too low. Avoid formation of hydrate particles within a certain pipe length.

Table 1. Experimental Data

initial pressure (MPa)	mass flow (kg/h)	temperature (K)	induction time (min)
4.1	1200	270.15	120.67
5.0	1200	270.15	90.33
6.0	1200	270.15	84.27
4.1	1500	274.15	208.67
5.0	1500	274.15	123.80
6.0	1500	274.15	76.13

2.2.2. Influence of Different Pressures on Gas Consumption. Figure 4 showed the variation of gas consumption

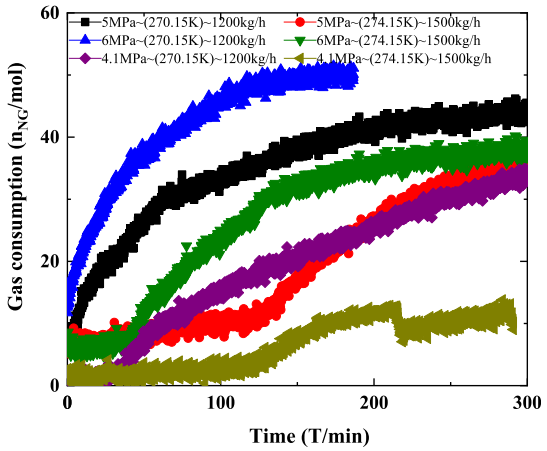

Figure 4. Influence of different initial pressures on gas consumption (4.1, 5, and 6 MPa).

in the hydrate mass formation stage at different initial pressures (4.1, 5, and 6 MPa) under the same temperature and mass flow. During the induction period, gas consumption was mainly dissolved gas, and the consumption rate was not obvious. Therefore, the following would focus on analyzing the variation rule of gas consumption during the stage of hydrate rapid growth. Due to the rapid formation of hydrate, a large amount of gas was consumed, so the gas consumption sharply increased, the growth rate was obviously accelerated. When the temperature was 274.15 K and the flow rate was 1500 kg/h, the gas consumption increased with the increase of the initial pressure. The same rule could still be obtained by changing the external temperature and the initial flow rate. At 1200 kg/h, the gas consumption at pressure 6 MP was twice that at 4 MPa, and at 1500 kg/h, the gas consumption at pressure 6 MP was three times that at 4 MPa. The explanation for this phenomenon was that the when the initial pressure increased, the driving force increased, and the hydrate formation rate was faster within the same time, so the final gas consumption was greater. It was also verified that there was no direct relationship between the gas consumption and the length of induction time.

As shown in Figure 5, the gas consumption data under the condition of 6 MPa to 270.15 K to 1200 kg/h were nonlinear fitted and the first derivative of the obtained fitting curve was taken, and the change of gas consumption rate in the rapid growth stage could be obtained, which showed a trend of first

https://doi.org/10.1021/acsomega.1c05127
ACS Omega 2022, 7, 599−616

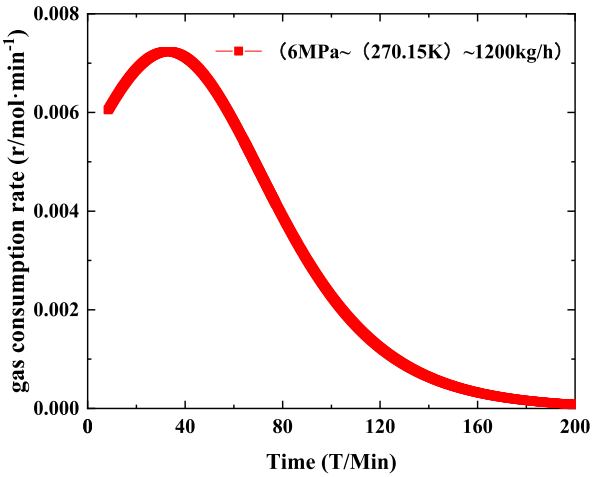

Figure 5. Variation trend of the gas consumption rate (6 MPa to 270.15 K to 1200 kg/h).

rise and then declined on the whole. The peak value of the gas consumption rate was reaching 0.0075. The main reason was that hydrate growth was controlled by driving force factors such as coolness and supersonic saturation at the early stage, and the effect of mass and heat transfer was small. However, in the stage of hydrate rapid formation, although the gas consumption rate was controlled by the intrinsic dynamics at the beginning, and the growth rate showed an upward trend, however, in the stage of hydrate rapid formation, with the growth and aggregation of the hydrate, mass and heat transfer gradually occupied the dominant position, leading to a gradual decline in the gas consumption rate, and finally tended to be stable. The study of Wu[55] showed that the hydrate formation rate in the experiment with an initial pressure of 4 MPa was about 1.5 times that of the experiment with an initial pressure of 3 MPa, which was the same as the experimental result.

2.2.3. Influence of Different Pressures on Hydrate Volume Fraction. Figure 6 showed the changes of hydrate volume fraction at different initial pressures (4.1, 5, and 6 MPa) under the same temperature and mass flow. It could be seen from the figure that the change rule of hydrate volume fraction with initial pressure was consistent with gas consumption but contrary to the change of induction time. Under the condition

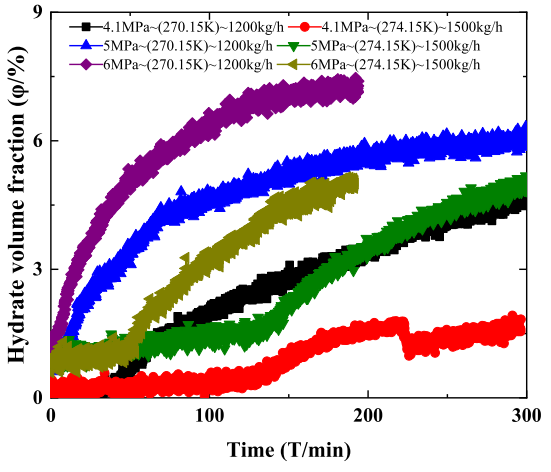

Figure 6. Influence of initial pressure on hydrate volume fraction (4.1, 5, and 6 MPa).

of 6 MPa to 270.15 K to 1200 kg/h, the hydrate volume fraction reached the maximum, up to 7.47%, about 2.13 times of the volume fraction under 4.1 MPa; the hydrate volume fraction at 4.1 MPa to 274.15 K to 1500 kg/h was about 1.7%, which was 1/3 of that under the same condition of 6 MPa. On the one hand, increasing the initial pressure could accelerate the formation rate of hydrate and shorten the induction period. On the other hand, by increasing gas consumption and hydrate volume fraction, the slurry viscosity and pressure drop in the pipe were changed. Figure 7 showed the changing rules of flow pressure drop and slurry viscosity with hydrate volume fraction.

Figure 7 showed that the pressure-drop and apparent viscosity increased within a certain range with the increase of the hydrate volume fraction and the slurry gradually transformed into non-Newtonian fluids, which aggravated the risk of pipe plugging. When the hydrate volume fraction increased to the critical value, the pipeline was blocked, and the pressure-drop and apparent viscosity decreased. The hydrate volume fraction was increased with the increase of initial pressure; therefore, the risk of pipe plugging increased with the increase of initial pressure. This conclusion was the same with Li[56] et al. that gas hydrate plugging was more likely to occur in pipelines under high pressure in oil−water systems.

Hydrate formation would change not only the pressure drop and apparent viscosity of the slurry but also the flow pattern of the slurry. Ding[57] et al. studied hydrate slurry flow characteristics before and after hydrate formation at different gas−liquid flow rates using the high-pressure flow loop. The migration trend of the multiphase flow pattern was obvious before and after hydrate formation. In the presence of hydrate particles, the slurry was easier to transition from stratified flow to slug flow. Therefore, in order to ensure the safe operation of the mixed transportation pipeline, the initial pressure should not be too high to lead to the increase of hydrate volume fraction, resulting in the increase of pressure drop, slurry viscosity, and a change in flow patterns. Ultimately, increasing the blocking risk (Table 2).

2.3. Influence of Different Flow Rates on the Growth Kinetics of Hydrate. *2.3.1. Influence of Different Flow Rates on the Induction Period of Hydrate Formation.* Figure 8 showed the variation of the induction time of NGH with flow rate. The experimental data are shown in Table 3. Under the condition of initial pressure of 5 MPa and temperature of 274.15 K, the induction time at the flow rate of 550 kg/h was 135.2 min, which was about 5.33% shorter than that at the flow rate of 1500 kg/h, which was 128 min. When the temperature was reduced to 272.15 K, the induction time corresponding to the flow rate of 1300 kg/h was shortened by 12.9% compared with that of the flow rate of 550 kg/h. Under the condition of initial pressure of 6 MPa and temperature of 274.15 K, the induction time at the flow rate of 550 kg/h was 102.53 min, which was shortened by about 13.91% compared with the corresponding induction time of 88.27 min at 1500 kg/h. When the temperature dropped to 272.15 K, the induction time corresponding to the flow rate of 1300 kg/h was shortened by about 17.75% compared with the flow rate of 550 kg/h. The lower the temperature, the shorter the induction period. From this, it could be concluded that the induction time was shortened with the increase of flow rate. The main reason was that with the increase of flow rate, the turbulence degree of the slurry was higher, the nucleation points were more, and the mass transfer was strengthened, so the induction

https://doi.org/10.1021/acsomega.1c05127
ACS Omega 2022, 7, 599−616

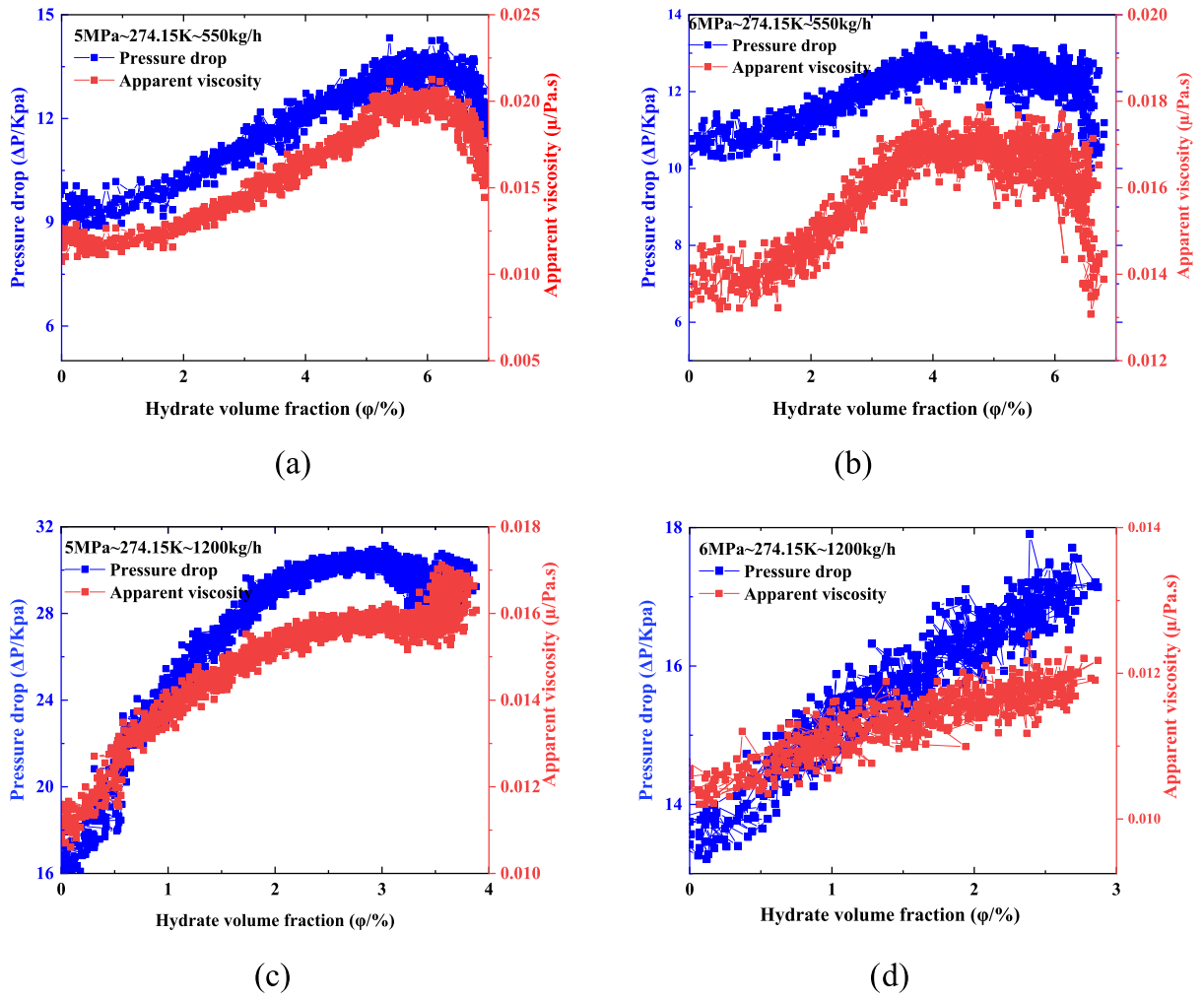

Figure 7. Variation of pressure drop and apparent viscosity under different hydrate volume fractions.

Table 2. Experimental Parameters

initial pressure (MPa)	initial flow (kg/h)	temperature (K)	induction time (min)
5	550	274.15	135.2
5	1500	274.15	128
5	550	272.15	86.8
5	1300	272.15	75.06
6	550	274.15	102.53
6	1500	274.15	88.27
6	550	272.15	80
6	1300	272.15	65.8

period was shortened. However, this was different from the tendency that induction period decreased first and then increased with the increase of flow rate obtained by Li[58] et al. in the oil-in-water system, which could be explained as follows: the increase of the flow rate aggravated the frictional heat generation between the fluid and wall and between the fluid and fluid, weakened the cooling effect of the experimental system, inhibited the crystallization and nucleation of hydrate, and prolonged the hydrate induction period.

2.3.2. Influence of Different Flow Rates on Gas Consumption. Figure 9 showed the changes of gas consumption in the four groups under the same pressure and different flow rates. As can be seen from Figure 10, during the rapid growth stage of the hydrate, gas consumption rose sharply, and the consumption rate is shown in Figure 10, showing a trend of the first rise and then decline. The peak value of the consumption rate was 0.015. The maximum gas consumption was 58 mol at 5 MPa to 272.15 K to 550 kg/h, which was 1.29 times of that at 1300 kg/h. Under the condition of 5 MPa to 270.15 K, the gas consumption of 550 kg/h was 2.33 times that of 1300 kg/h. Under the pressure of 6 MPa, the similar experimental law could still be obtained. It indicated that the gas consumption decreased with the increase of the flow rate. The explanation for this conclusion was that the increase of the flow rate led to the decrease of the heat transfer efficiency in the tube, and the heat released from hydrate generation was not easy to be taken away, the heat transfer was limited, thus resulting in the decrease of gas consumption. It was also verified that the large flow rate could not only shorten the induction period but also inhibit the formation of hydrate in the later stage. In the actual mixed transportation pipeline, it was necessary to control the flow rate not to be too high to shorten the hydrate induction period, accelerating the hydrate generation rate within the limited pipe length. In addition, the flow rate should not be too low, resulting in increased gas consumption in the hydrate growth stage, and eventually increased hydrate volume fraction, leading to the risk of pipe blocking. Therefore, reasonable

https://doi.org/10.1021/acsomega.1c05127
ACS Omega 2022, 7, 599−616

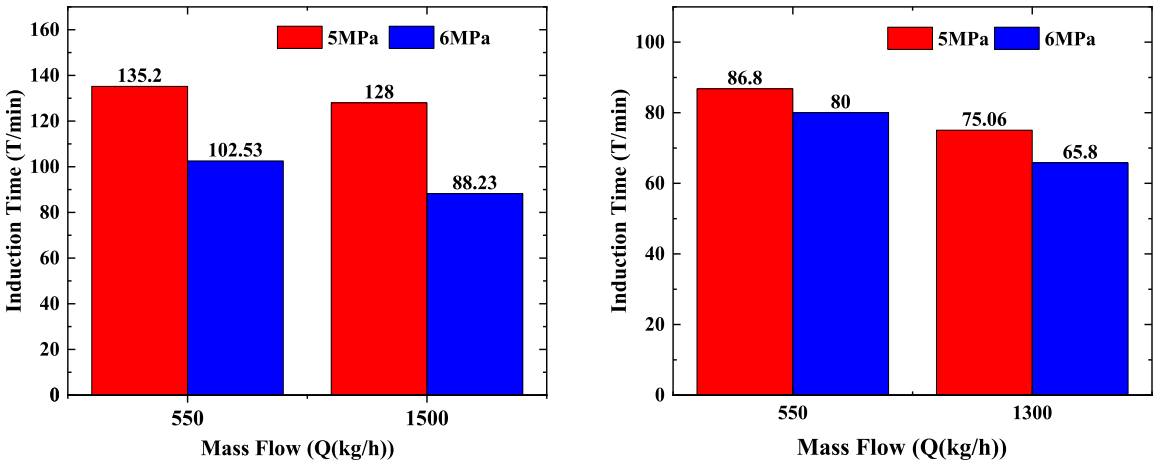

Figure 8. Influence of different initial flows on induction time.

Table 3. Experimental Data

initial pressure (MPa)	water cut (%)	induction time (min)
5	15	150
5	20	64
6	15	68.4
6	20	58.53
7	15	63.73
7	20	50.4

flow rate was an important factor for safe operation of the pipeline.

2.3.3. Influence of Different Flow Rates on Hydrate Volume Fraction. Figure 11 showed the variation of hydrate volume fraction in two groups at different flow rates and same initial pressure. As can be seen from the figure, the change of hydrate volume fraction at different flow rates was consistent with the change rule of gas consumption, which rose first and then tended to be stable in the stage of hydrate mass generation. Under the condition of 6 MPa to 274.15 K, the hydrate volume fraction corresponding to 1500 kg/h was the smallest, which was about 1.25 times of 550 kg/h. While under the condition of 5 MPa to 272.15 K, the hydrate volume fraction of 550 kg/h was the largest, which was about 3/4 of that of 1300 kg/h. This also showed that the factors that control hydrate growth during the growth stage were different; in the early stage, it was controlled by intrinsic kinetics and the growth rate was accelerated. With the formation of hydrate, it was mainly affected by mass and heat transfer. However, the restriction of mass and heat transfer was more obvious at a higher flow rate, so the final hydrate volume fraction increased.

This conclusion was consistent with the effect of flow rate on hydrate volume fraction simulated by Wang[59] et al. based on OLGA, the peak value of hydrate volume fraction increased with the increase of flow rate. When the flow rate reached 4500 m^3/d, no hydrate was formed in the pipeline.

2.4. Influence of Different Water Cuts on the Hydrate Growth Kinetics. *2.4.1. Influence of Different Water Cuts on the Induction Period.* Figure 12 showed the influence of different water cuts on the hydrate induction time. The experimental data are shown in Table 4. As can be seen from the figure, under the same pressure of 5 MPa, the induction time of 20% water cut was 64 min, which was 57.3% shorter than the induction time of 150 min under 15% water cut, the induction time at 6 and 7 MPa was shortened by 13.99 and 20.92%, respectively. Therefore, with the increase of water cut, the induction time shortened. This phenomenon could be explained as follows: the increase of water cut made the medium in the tube mix evenly, the surface area of oil−water and gas contact increased, and then, the nucleation points increased, leading to the acceleration of the formation rate, so the macroscopic induction time was shortened. In view of this, in the actual mixed pipeline, it should be guaranteed that the water cut was nearly possible to be low. However, the conclusion was not consistent with the conclusion of Turner,[60] who believed that the induction time presented a V-shape with the increase of water cut. The explanation for this was that the dissolved gas in unit liquid volume decreased with the increase of water cut. In the process of hydrate nucleation and growth, the mass transfer of gas was limited. Thus, inhibiting the formation of hydrate.

2.4.2. Influence of Different Water Cuts on Gas Consumption. Figures 13 and 14, respectively, showed the influence rules of different water cuts on gas consumption and consumption rate. As can be seen from Figure 13, with the increase of water cut, the gas consumption rose rapidly at first and then became stable. At the same pressure, the gas consumption increased with the increase of water cut. Under 5 MPa, the gas consumption under 20% water cut was 1.5 times that of 15% water cut, and under 6 MPa, the gas consumption under 20% water cut was 1.09 times that of 15% water cut. The first-order derivative of the gas consumption at different water cuts under 6 MPa could get the change of the gas consumption rate. As shown in Figure 14, in the rapid formation stage of hydrate, the gas consumption rate first increased and then decreased. The peak value of the gas consumption rate was increased by the increase of water cut, and the time needed to reach the peak value decreased with the increase of water cut. The reasons for the above phenomena could be summarized as follows: the higher the water cut, the larger the interface surface of the oil−water phase, the mass transfer would be enhanced under the same pressure, so the growth rate would increase. The decrease of the rate also indicated that the hydrate was mainly affected by the mass and heat transfer during the late growth period.

2.4.3. Influence of Different Water Cuts on Hydrate Volume Fraction. Figure 15 showed the influence rule of different water cuts on hydrate volume fraction. The variation trend was roughly the same as that of gas consumption, rising

https://doi.org/10.1021/acsomega.1c05127
ACS Omega 2022, 7, 599−616

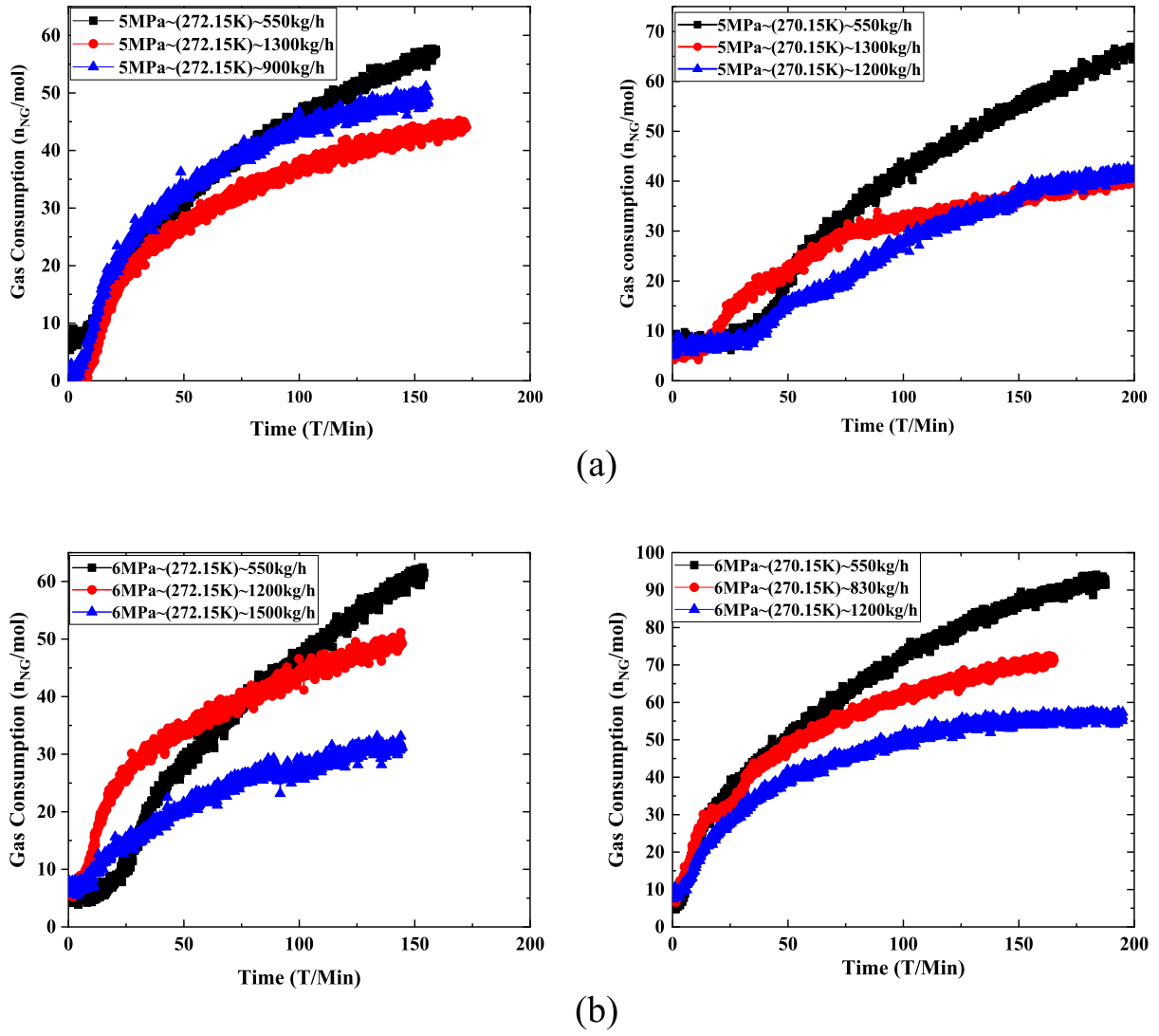

Figure 9. Influence of different initial flow rates on gas consumption (a: 5 MPa; b: 6 MPa).

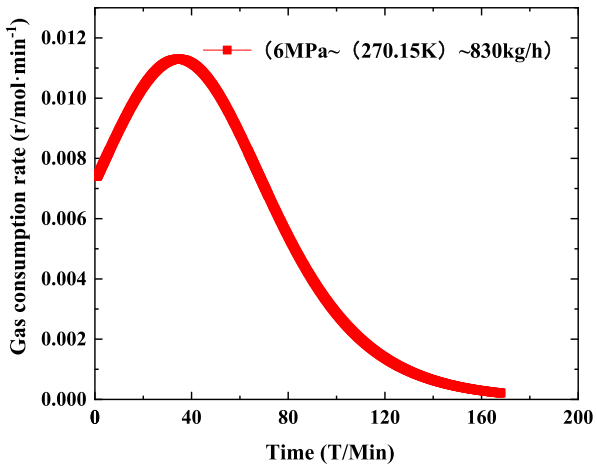

Figure 10. Variation of gas consumption rate (6 MPa to 270.15 K−830 kg/h).

first and then tending to be stable. At the same pressure of 5 MPa, the hydrate volume fraction with 15% water cut was higher than that with 20% water cut, and the same conclusion was reached at 6 and 7 MPa. In addition, the hydrate volume fraction reached the maximum under the condition of 7 MPa−20%, up to 16%, indicating that the hydrate volume fraction increased with the increase of water cut. In the above studies, it had been concluded that the pressure-drop and apparent viscosity increased with the increase of hydrate volume fraction. Therefore, in the actual mixed pipeline, the water cut should not be too high to ensure that the hydrate volume fraction was not too large, resulting in pressure drop and apparent viscosity increase, and eventually causing pipeline blockage.

3. EMPIRICAL FORMULA OF INDUCTION TIME WAS ESTABLISHED IN THE OIL−WATER EMULSION SYSTEM

According to the above research, the induction time was affected by the initial pressure, flow rate, and water cut. In view of this, this paper adopted the "standard regression coefficient method" to conduct sensitivity analysis on the influence of the initial pressure, flow rate, and water cut on the induction time in order to determine the level of sensitivity to each factor.

The standard regression coefficient method was used for sensitivity analysis, and the equations were as shown in eqs 3−11. The dependent variable Y was affected by the

https://doi.org/10.1021/acsomega.1c05127
ACS Omega 2022, 7, 599−616

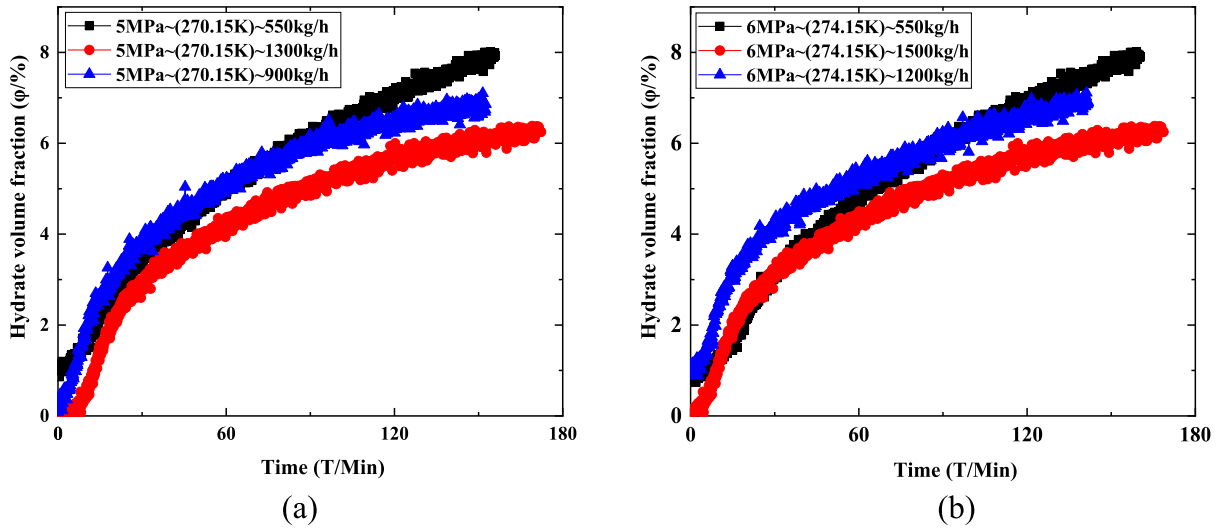

Figure 11. Influence of different initial flow rates on hydrate volume fraction (a: 5, b: 6 MPa).

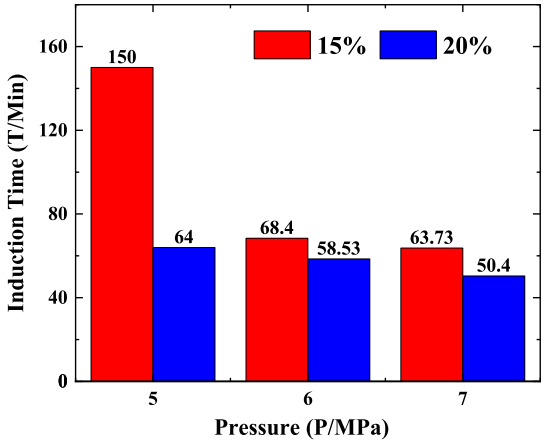

Figure 12. Influence of different water cuts on the induction time (5; 6; and 7 MPa).

Table 4. Experimental Parameters

initial pressure (MPa)	flow rate (kg/min)	water cut (%)	induction time (h)	calculated value (h)	error (%)	average error (%)
4.1	20	15	0.84	1.0840	29.05	27.10
5	20	15	0.71	0.8500	19.72	
6	20	15	0.63	0.5900	6.35	
4.1	9.17	15	2.48	1.5172	36.25	
5	9.17	15	2.25	1.2832	40.32	
6	9.17	15	1.71	1.0232	40.16	
5	14.17	15	2.5	1.0832	48.42	
6	14.17	20	1.07	0.9732	9.05	
7	14.17	20	0.84	0.7132	15.10	
4	19	10	1.98	1.0000	49.49	
4.5	16.7	10	0.76	0.9620	26.58	
5	19	10	0.7	0.7400	5.71	

independent variables X_1, X_2, X_3,..., X_m, and a total of n experiments were carried out.

$$I_{ij} = \sum_{(k=1)}^{n} (X_{ik} - \bar{X}_1)(X_{jk} - \bar{X}_1) \tag{3}$$

$$I_{i0} = \sum_{k=1}^{n} (X_{ik} - \bar{X}_i)(X_k - \bar{Y}) \tag{4}$$

$$I_{00} = \sum_{k=1}^{n} |Y_k - \bar{Y}|(i, j = 1,2, \ldots, m) \tag{5}$$

$$(\bar{X}_i) = 1/n \sum_{(k=1)}^{n} X_{ik}(i, j = 1,2, \ldots, m) \tag{6}$$

$$\bar{Y}_i = 1/n \sum_{(k=1)}^{n} Y_k(k = 1,2, \ldots, n) \tag{7}$$

X_{ik} is the value of the independent variable.X_i in the k test and Y_k is the result of the dependent variable Y in the k test. If there was a linear relationship between Y andX_i, the regression equation was as follows

$$Y = a + b_1x_1 + b_2x_2 + \ldots + b_mX_m \tag{8}$$

Among them

$$\sum_{(k=1)}^{n} I_{ij}b_j = I_{i0}(i = 1,2, \ldots, m) \tag{9}$$

$$a = \bar{Y} - \sum_{i=1}^{m} b_i\bar{X}_i \tag{10}$$

The standard regression coefficient was:

$$\bar{b}_i = b_i\sqrt{\frac{I_{ii}}{I_{00}}} \tag{11}$$

The greater the absolute value of the standard regression coefficient, the greater the influence of X_i on Y.

Some experimental parameters are shown in Table 4. The initial pressure, flow rate, and water cut were taken as independent variables X_1, X_2, and X_3, respectively, and the induction time was the dependent variable Y which could be calculated from eqs 3−11

$$\bar{X}_1 = 5.14,\ \bar{X}_2 = 15.39,\ \bar{X}_3 = 14.58,\ \bar{X}_4 = 1.05$$

https://doi.org/10.1021/acsomega.1c05127
ACS Omega 2022, 7, 599−616

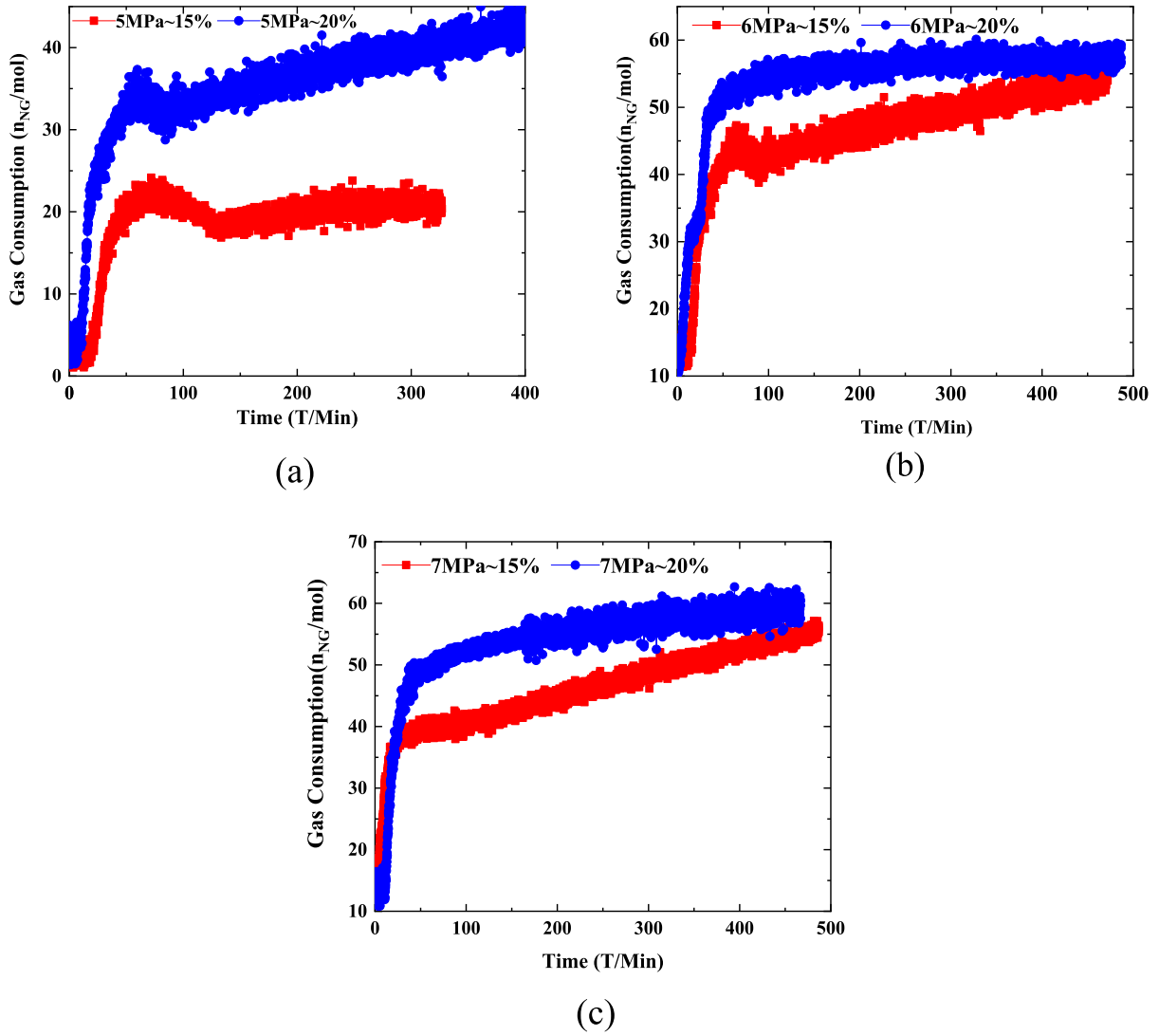

Figure 13. Influence of different water cuts on gas consumption (a: 5, b: 6, and c: 7 MPa).

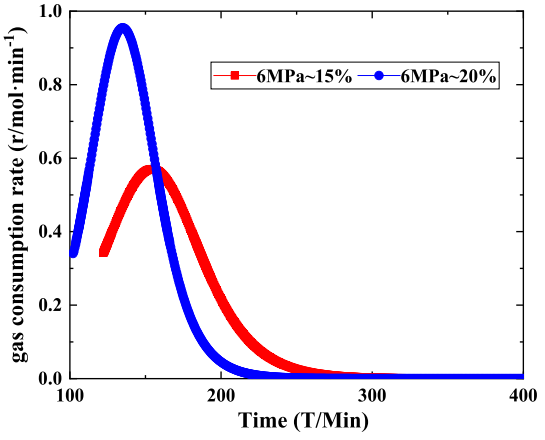

Figure 14. Influence of different water cuts on gas consumption rate (6 MPa).

$I_{00} = 3.92,\ I_{10} = -1.8428,\ I_{20} = -5.8118,\ I_{30} = -2.3916$

$I_{11} = 9.4112,\ I_{22} = 212.067,\ I_{33} = 122.9168$

$I_{12} = I_{21} = -7.7306,\ I_{13} = I_{31} = 22.7504,\ I_{23} = I_{32} = 54.8332$

List the equations to solve the regression coefficient

$$-1.8428 = 9.4112b_1 - 7.7306b_2 + 22.7504b_3$$

$$-5.8118 = -7.7306b_1 - 212.067b_2 - 54.8332b_3$$

$$-2.3916 = 22.7504b_1 - 54.8332b_2 + 122.9168b_3$$

The coefficients of the solution were

$b_1 = -0.26,\ b_2 = -0.04,\ b_3 = -0.03.$

The standard regression coefficient was finally obtained

$$\bar{b}_1 = b_1\sqrt{\frac{I_{11}}{I_{00}}} = -0.3973,\ \bar{b}_2 = b_2\sqrt{\frac{I_{22}}{I_{00}}} = -0.2456,\ \bar{b}_3 = b_3\sqrt{\frac{I_{33}}{I_{00}}} = -0.07061$$

Could be seen from the results $|\bar{b}_1| > |\bar{b}_2| > |\bar{b}_3|$, so the initial pressure had the greatest influence on the induction period, the

https://doi.org/10.1021/acsomega.1c05127
ACS Omega 2022, 7, 599−616

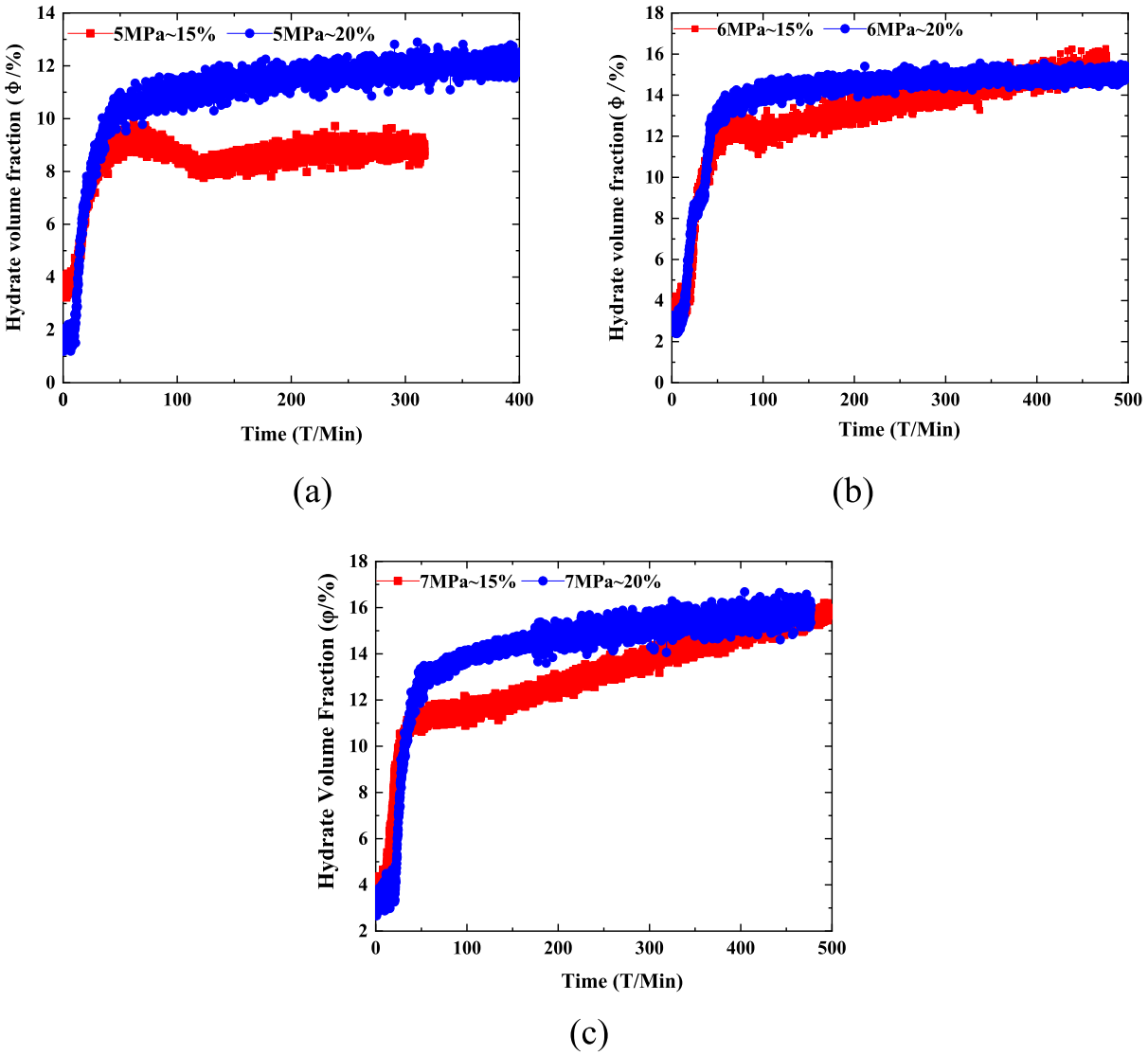

Figure 15. Influence of different water cuts on hydrate volume fraction (a: 5, b: 6, and c: 7 MPa).

flow rate was the second, and the influence of water cut was the least.

Furthermore, the coefficient of the constant term was obtained by eq 12 as follows

$$a = \overline{Y} - \sum_{i=1}^{m} b_i \overline{X}_i = 2.5 \tag{12}$$

The constant term and regression coefficient were substituted into $Y = a + b_1x_1 + b_2x_2 + ...b_mx_m$ to obtain the functional relationship between the induction time and each variable, as shown in eq 13. It should be noted here that the calculation data of the whole parameters came from the experiment conducted in the flow loop. Therefore, when using this formula to predict induction time, it was necessary to combine different actual loop correlation conditions and add relevant correction coefficients for correction.

$$T_{ind} = 2.70 - 0.2564P - 0.03339Q + 0.01261\alpha \tag{13}$$

By comparing the calculated values with the experimental values, it was found that most of the relative errors were within 30% and the average error was 27.1%. Therefore, the empirical formula could better predict the induction time in the oil–water emulsion.

Above all, combining various factors influence the hydrate formation induction period in the actual mixed pipeline, and to prevent the hydrate formation from the pipeline blockage, reducing the pressure was the most effective measure. Second, the induction period could be prolonged by reducing the flow rate and water cut. These measures could reduce the probability of hydrate generated within a limited length, so as to ensure the security of the pipeline.

The empirical formula of hydrate induction period given in this work involved many parameters, which were all key parameters affecting the hydrate induction time, so it could better describe the NGH induction time of oil-in-water emulsion. The hydrate induction period model was applied to the system with high flow rate (1940 kg/h) and low pressure (3.2 MPa) established by LV[61] et al. The experimental results showed that the hydrate formation induction time was 0.71 and 1.50 h, respectively, compared with 0.90 and 1.58 h calculated by the hydrate induction period model. The relative errors were 26.76 and 5%,

https://doi.org/10.1021/acsomega.1c05127
ACS Omega 2022, 7, 599−616

Table 5. Distribution of the Induction Period under Different Experimental Systems

researchers	methods	factors	induction period (h)
Talaghat[62] (2013)	flow loop	the effects of kinetic inhibitors PVP, L-tyrosine, and PVCapD on hydrate induction time	0.26−12.85
Talaghat[63] (2014)	flow loop	the effects of PVP and L-tyrosine bidynamic inhibition exist simultaneously on hydrate induction time	0.67−7.5
Wang[64] (2014)	flow loop	the effects of temperature, pressure, and gas phase/liquid phase conversion velocity on the induction period of gas hydrate	0.067−0.75
Lv[65] (2014)	flow loop	the effects of subcooling degree, supersaturation, flow rate, water cut, and concentration of polymerization inhibitor on the induction period of gas hydrate	0.25−4
WANG[32] (2016)	reactor	the effects of "memory effect", experimental temperature, water cut, and porous media environment on the induction period of gas hydrate	0.33−23.33
Moraveji[66] (2017)	reactor	the effects of surfactants SDS, HTAB, and Triton X-405 on the induction period of methane hydrate	0.37−5.42
Shi[22] (2018)	flow loop	the effects of wax crystal on the induction period of gas hydrate	6.47
Lan[67] (2020)	reactor	The effects of solid particles on the induction time of methane hydrate	0.5−2.2
Zhang[68] (2020)	reactor	the effects of surfactants CPDA, SDS, CTAB, and HTAB on the induction time of methane hydrate	0.45−0.75
Wu[69] (2021)	reactor	the effects of surfactants SDS, rhamolipid, Tween 80, and triton X-10 on induction period of methane hydrate	0.35−10.0

indicating that the induction period model could be better applied to systems with high flow rate and low pressure.

However, the hydrate induction time would be shortened or extended due to different experimental equipment or systems. Table 5 listed the induction period distribution of different experimental systems. As can be seen from Table 5, due to different factors considered in the experimental system, the induction period was widely distributed, ranging from a few minutes to dozens of hours. In view of this, temperature, pressure, flow rate, water cut, gas phase composition, kinetic inhibitors, porous media environment, and so forth could be classified and combined in the future to improve the systematization of qualitative influencing factor analysis during the induction period.

4. ESTABLISHMENT OF HYDRATE VOLUME FRACTION MODEL IN THE OIL−WATER EMULSION SYSTEM

4.1. Analysis of Influencing Factors of Hydrate Volume Fraction Based on the Gray Correlation Method. The hydrate volume fraction had a direct impact on the security of the pipeline, so it was necessary to carry out sensitivity analysis of hydrate volume fraction. In this paper, the gray correlation method was used to analyze the influencing factors of hydrate volume fraction. Some selected experimental data are shown in Table 6. According to the above research results, initial pressure, flow rate, and water cut all had an impact on the hydrate volume fraction. Indicators such as initial pressure, flow rate, and water cut were selected as the comparison sequence, denoted as $X_1(k)$, $X_2(k)$, and $X_3(k)$, respectively. The hydrate volume fraction was taken as the reference sequence, denoted as $X_0(k)$.

Table 6. Experimental Data

initial pressure (MPa) $X_1(k)$	flow rate (kg/min) $X_2(k)$	water cut (%) $X_3(k)$	hydrate volume fraction (%) $X_0(k)$
4.1	20.00	15	2.49
5	20.00	15	4.97
6	20.00	15	7.12
6	9.17	15	11.95
6	13.83	15	9.03
6	20.00	15	7.23
5	23.33	10	3.82
5	23.33	15	6.39
5	23.33	20	12.78

The minimization production method was adopted to normalize the reference sequence and comparison sequence, in which $X_i(k)$ was the comparison sequence and $X_i(1)$ was the first value of the sequence. The specific eq 14 was as follows

$$X_i'(k) = \frac{X_i(k)}{X_i(1)} \qquad i = 1,2,3\ldots, n \tag{14}$$

The original data were optimized according to the normalization treatment equation and a new sequence was obtained, as shown in Table 7.

When the sequence was at time t, $\Delta_{i(t)} = |X_0'(t) - X_i'(t)|$ was the difference sequence, representing the absolute difference between each point on the curve of comparison sequence $X_i'(k)$ and that of reference sequence $X_0'(t)$.The absolute difference of the original data was calculated, and the specific data obtained are shown in Table 8.

eq 15 of correlation coefficient was as follows

$$\varphi_{i(t)} = \frac{\min\{\min \Delta_{i(t)}\} + \{K \max \max \Delta_{i(t)}\}}{\Delta_{i(t)} + K \max\{\max \Delta_{i(t)}\}} \tag{15}$$

The absolute difference value was substituted into the formula to calculate the correlation degree between comparison sequence and reference sequence, where $K = 0.5$. The calculation results are shown in Table 9.

According to the basic principle of gray correlation analysis, the correlation coefficients at each moment were concentrated into a value, that is, the average value was calculated as the quantitative representation of the correlation degree between the comparison sequence and reference sequence. The calculation eq 16 was as follows

$$r_i = \frac{1}{N}\sum_{k=1}^{n} \varphi_i(t) \tag{16}$$

The indexes were sorted according to the correlation degree, and the results are shown in Table 10.

The result by the correlation degree was $r_1 > r_2 > r_3$, showing that the hydrate volume fraction had the closest relationship

https://doi.org/10.1021/acsomega.1c05127
ACS Omega 2022, 7, 599−616

Table 7. Parameters after Normalization of Indicators

normalized parameters	data								
$x_0'(k)$	1	2.00	2.86	4.80	3.63	2.90	1.53	2.57	5.13
$x_1'(k)$	1	1.22	1.46	1.46	1.46	1.46	1.22	1.22	1.22
$x_2'(k)$	1	1	1	0.46	0.69	1	1.17	1.17	1.17
$x_3'(k)$	1	1	1	1	1	1	0.67	1	1.33

Table 8. Absolute Difference between the Reference Sequence and Comparison Sequence

absolute difference	data								
$\Delta_{1(t)}$	0	0.78	1.4	3.34	2.17	1.44	0.31	1.35	3.91
$\Delta_{2(t)}$	0	1	1.86	4.34	2.94	1.9	0.36	1.4	3.96
$\Delta_{3(t)}$	0	1	1.86	3.8	2.63	1.9	0.86	1.57	3.8

Table 9. Gray Correlation Coefficient Statistics of Reference Sequence and Comparison Sequence

correlation coefficient	data								
φ_1	1	0.71	0.58	0.37	0.47	0.58	0.86	0.59	0.33
φ_2	1	0.68	0.54	0.33	0.42	0.53	0.86	0.61	0.35
φ_3	1	0.66	0.51	0.33	0.42	0.50	0.69	0.55	0.33

Table 10. Rank of Correlation Degree

indicators	correlation degree r_i	rank
$X_1(k)$	0.61	1
$X_2(k)$	0.59	2
$X_3(k)$	0.55	3

with the initial pressure, followed by the flow rate and then the water cut. In conclusion, the initial pressure in the oil−water system was the biggest factor affecting the hydrate volume fraction. In order to ensure that the multiphase mixed transportation pipeline in the system did not clog, the initial pressure should not be too high.

4.2. Formula of Maximum Hydrate Volume Fraction in the Pipe. Based on the sensitivity analysis of the gray correlation method, it was concluded that the pressure and flow rate were the main factors affecting the maximum volume fraction in the pipe. In view of this, the P/Q value was taken as the abscissa and the maximum volume fraction in the pipeline as the ordinate to establish the prediction formula of the maximum hydrate volume fraction in the oil−water emulsion system. $a = 7.907$, $b = 19.136$, $c = 35.272$ were determined by the regression of experimental data. Therefore, the final prediction model of the maximum hydrate volume fraction in the oil−water emulsion was as follows: $Y = 7.907(1 - e^{-19.136(P/Q)})^{35.272}$. The relative error between the experimental value and the calculated value was within 30%, and the variation trend of the predicted value and the experimental value was roughly the same, and at the same time, this model was applied to the oil−water emulsion system established by SHI,[32] and the relative error was 11.85%, which indicated that the established model could predict the maximum volume fraction in the pipe of oil−water emulsion system as well (Figure 16).

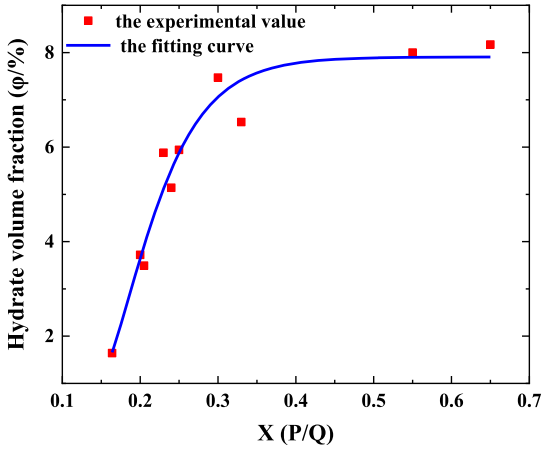

Figure 16. Curve of maximum volume fraction changing with $X(P/Q)$.

5. CONCLUSIONS AND SUGGESTIONS

In this paper, an experiment on the NGH growth kinetics in an oil−water emulsion system was carried out by means of a high-pressure hydrate flow loop. The influence of pressure, flow rate, and water cut in the induction time, volume fraction, and gas consumption were studied. The following conclusions were obtained:

(1) The formation of O/W NGH could be divided into three stages, including the induction period, the stage of mass generation, and the steady flow stage of the slurry. The rapid formation of hydrate was marked by a sudden rise in temperature and pressure drop and a rapid rise in gas consumption and hydrate volume fraction.

(2) The induction time of NGH decreases with the increase of initial pressure, initial flow rate, and water cut, and the change of gas consumption and hydrate volume fraction was synchronized, increased with the increase of initial pressure and water cut and decreased with the increase of the initial flow rate. This indicated that low pressure, low flow rate, and low water cut could effectively prolong the induction period.

(3) The apparent viscosity and flow pressure drop of hydrate slurry increased within a certain range with the increase of hydrate volume fraction, which aggravated the risk of pipe plugging. Moreover, hydrate volume fraction increased with the increase of initial pressure and water cut. Therefore, it was necessary to reduce the

https://doi.org/10.1021/acsomega.1c05127
ACS Omega 2022, 7, 599−616

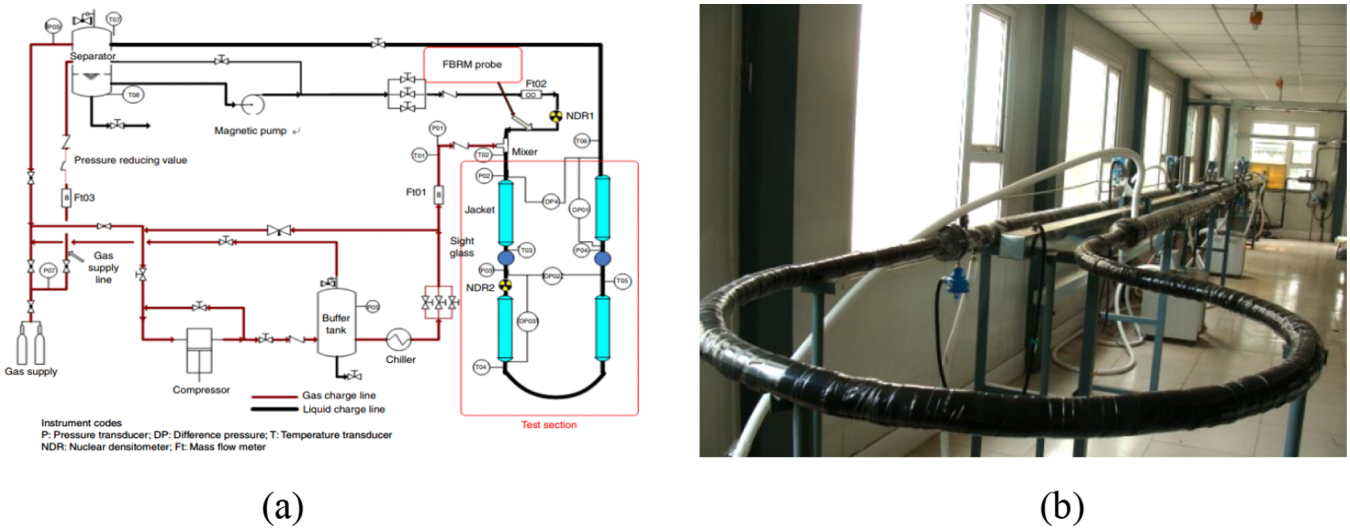

Figure 17. Schematic diagram of the high-pressure hydrate flow loop (a: schematic diagram; b: physical diagram)[51] (photograph courtesy of Shi. Copyright 2021).

initial pressure and water cut to ensure that the hydrate volume fraction should not be too high. The initial growth of hydrate was mainly controlled by intrinsic dynamics, and the later growth was mainly controlled by mass and heat transfer. Therefore, the study on the growth kinetic characteristics of hydrate must be carried out from both thermodynamics and kinetics.

(4) Sensitivity analysis showed that initial pressure played a major role in the induction period, while water cut had the weakest effect. An empirical formula for the induction time in oil−water system was established. Based on the gray correlation method, the sensitivity analysis of the hydrate volume fraction was carried out. The relationship between the hydrate volume fraction and the initial pressure was the closest, followed by the flow rate, and the water cut was the least. The empirical formula of the hydrate volume fraction in the oil−water system was established. The applicability of the two empirical formulas was good.

(5) In the future of NGH growth dynamics study, explore the suggestions from the following aspects: analyze the influence of pressure, flow rate, water cut, and so forth on the microscopic characteristics of particles, and use advanced microscopic observation equipment or numerical simulation software to conduct microscale research in order to obtain a more perfect growth dynamic characteristic. The establishment of empirical formula should classify and combine the influencing factors to improve the systematic of the influencing factor analysis.

6. EXPERIMENTAL SECTION

6.1. Experimental Apparatuses and Materials. The experiment used the hydrate experiment loop of China University of Petroleum (Beijing) Oil and Gas Storage and Transportation Multiphase Flow Laboratory, which was composed of oil, gas, and water three-phase supply system, experimental pipe section, temperature control system, data acquisition system, and so forth. In addition, it was equipped with an online particle analyzer (FBRM), temperature controller, and other advanced experimental instruments. The main parameters of the loop were as follows: the design pressure was 0−15 MPa, design temperature was −20 to 80 °C, the loop length was 30 m, the inner diameter was 2.54 cm, and the wall thickness was 2.8 mm. The schematic diagram of the flow loop is shown in Figure 17.

The experimental materials were deionized water, −20# diesel, and natural gas of Shan Jing Line. The specific composition of natural gas is shown in Table 11. The experiment adopted a control variable method. The anti-agglomerant was combined with hydrate antiagglomerant.

Table 11. Composition of Natural Gas

composition	mole percent	composition	mole percent
C_1	89.02	nC_6^+	0.01
C_2	3.07	CO_2	0.89
C_3	3.06	CO	2.05
iC_4	0.33	N_2	1.53
iC_5	0.04		

The experimental pressure was selected as the high pressure below 10 MPa, mainly for the first reason that the design pressure of the experimental loop was 15 MPa, and the second reason was that the high-pressure range was closest to the conveying pressure of the Chinese offshore platform. The reason for selecting low water cut was to simulate the characteristics of low water cut in the early stage of exploitation of Marine mixed transportation pipelines. The flow rate was between 550 and 1500 kg/h because too low flow rate would affect the slurry flow, and too high flow rate would cause large energy consumption.

6.2. Experimental Steps and the Formation of Water-In-Oil Emulsions. Taking the operating conditions of 274.15 K temperature, 550 kg/h flow rate, 10% water cut, and 5 MPa pressure as an example, the experimental procedures and the formation of the water-in-oil emulsion were summarized.

(1) Opened the vacuum pump for 1 h to vacuum the whole experimental loop, making the vacuum degree reach 0.02 MPa.

(2) Added experimental media (7 L water and 70 L −20#diesel) to the charging hole of the separator by self-priming of the experimental loop.

https://doi.org/10.1021/acsomega.1c05127
ACS Omega 2022, 7, 599−616

(3) Turn on the data acquisition system and a low-temperature water bath and set the experimental temperature at 274.15 K. The magnetic pump was turned on, the oil−water mixture was stirred fully for about 3 h, and added an inhibitor. Started FBRM and PVM to data collection. When the number of particles recorded by FBRM in the range of the chords of each particle size was stable and it was obvious that a large number of droplets with uniform distribution could be observed by PVM. It was considered that the oil−water mixture had been fully shorn, forming a relatively stable oil-in-water emulsion.
(4) Opened the inlet valve, and when the natural gas in the high-pressure cylinder entered the experimental loop and reached the experimental pressure, opened the circulating pump, so that the gas−liquid mixture was fully mixed to achieve the dissolution balance.
(5) Cooled and turned on the data acquisition system to record the parameters (pressure, pressure drop, flow rate, temperature, gas consumption, etc.). When the temperature reached below the phase equilibrium temperature, the hydrate started to form.
(6) When the hydrate was basically formed and the pressure and temperature in the pipe remained stable, the system temperature was increased to make the hydrate decompose.

6.3. Calculation of Experimental Parameters. *6.3.1. Determination of Gas Consumption.* The gas consumption was determined by the difference of the molar amount of natural gas in any two moments, as shown in eq 17.

$$n_{NG,t} = (n_{NG,l,(t=0)} + n_{NG,g,(t=0)}) - (n_{NG,l,t} + n_{NG,g,t}) \quad (17)$$

In eq 17, $n_{NG,t}$ is the number of moles of natural gas consumed at time t; $n_{NG,g}$ is the number of moles of natural gas in the gas phase; and $n_{NG,l}$ is the number of moles of natural gas in the liquid phase, Subscript $t = 0$, t represented the experimental conditions at the initial time and at the time t, respectively.

6.3.2. Determination of Hydrate Volume Fraction. The formation of hydrate particles would change the flow characteristics of the slurry, and the flow parameters would also change accordingly. Therefore, the hydrate volume fraction was an important factor affecting the flow characteristics of the hydrate slurry. The calculation formula of the hydrate formation volume fraction is shown in eqs 18−21

$$\phi_{hyd,t} = \frac{V_{hyd,t}}{V_{hyd,t} + V_{Liq}} \quad (18)$$

$$\phi_t = \frac{V_{hyd,t}}{V_{hyd,t} + V_{Liq}} \quad (19)$$

$$V_{Liq} = \frac{(m_{H_2O,loop(t=0)} - \beta n_{NG,t} M_{H_2O})}{\rho_{H_2O}} \quad (20)$$

$$M_g = \frac{\sum N_i M_i}{N_i} \quad (21)$$

In eqs 18−21, ϕ_t is the hydrate volume fraction at time t; V_{Liq} is the remaining liquid volume in the tube at time t, m^3; $n_{NG,t}$ is the gas consumption at time t, mol; M_g and M_w are the average molar mass of natural gas and the molar mass of water, respectively, g/mol; ρ_H and ρ_{H_2O} are the densities of hydrate and water, kg/m;[3] β is the real water composite number of hydrate formation in the system (hydrate type was type II, and the real water composite number was about 5.67); N_i is the molar percentage of a certain component of natural gas; and M_i is the molar mass of a certain component of natural gas.

AUTHOR INFORMATION

Corresponding Authors

Xiaofang Lv − *Jiangsu Key Laboratory of Oil and Gas Storage & Transportation Technology, Changzhou University, Changzhou 213016, China; China Petroleum & Chemical Corporation Northwest Oilfield Branch, Petroleum Engineering Technology Research Institute, Urumqi 830011, China*; Phone: +86 0519-8329-0280; Email: lvxiaofang5@cczu.edu.cn, lvxiaofang5@126.com

Yang Liu − *Jiangsu Key Laboratory of Oil and Gas Storage & Transportation Technology, Changzhou University, Changzhou 213016, China*; Phone: +86 05 19-8329-0280; Email: chrisblack@foxmail.com

Authors

Jie Zhang − *Jiangsu Key Laboratory of Oil and Gas Storage & Transportation Technology, Changzhou University, Changzhou 213016, China*; orcid.org/0000-0002-5343-8124

Yi Zhao − *China Petroleum & Chemical Corporation Northwest Oilfield Branch, Petroleum Engineering Technology Research Institute, Urumqi 830011, China*

Jiawen Xu − *Jiangsu Key Laboratory of Oil and Gas Storage & Transportation Technology, Changzhou University, Changzhou 213016, China*

Qianli Ma − *Jiangsu Key Laboratory of Oil and Gas Storage & Transportation Technology, Changzhou University, Changzhou 213016, China*

Shangfei Song − *National Engineering Laboratory for Pipeline Safety/ MOE Key Laboratory of Petroleum Engineering/ Beijing Key Laboratory of Urban Oil and Gas Distribution Technology, China University of Petroleum-Beijing, Beijing 102249, China*

Shidong Zhou − *Jiangsu Key Laboratory of Oil and Gas Storage & Transportation Technology, Changzhou University, Changzhou 213016, China*; orcid.org/0000-0001-8468-1226

Complete contact information is available at: https://pubs.acs.org/10.1021/acsomega.1c05127

Notes

The authors declare no competing financial interest.

ACKNOWLEDGMENTS

This work was supported by the National Natural Science Foundation of China (grant nos. 51804046, 52004039, and 51974037); China Postdoctoral Science Foundation (grant no. 2021M693908); and the major project of universities affiliated to Jiangsu Province basic science (natural science) research (no. 21KJA440001). Supported by Jiangsu Qinglan Project.

NOMENCLATURE

$n_{NG,t}$ the number of moles of natural gas consumed at time t mol
$n_{NG,g}$ the number of moles of natural gas in the gas phase mol

https://doi.org/10.1021/acsomega.1c05127
ACS Omega 2022, 7, 599−616

$n_{NG,l}$ the number of moles of natural gas in the liquid phase mol
ϕ_t the hydrate volume fraction at time t
V_{Liq} the remaining liquid volume in the tube at time t m^3
$n_{NG,t}$ the gas consumption at time t mol
M_g the average molar mass of natural gas g/mol
M_w the molar mass of water g/mol
ρ_H the density of hydrate kg/m^3
ρ_{H_2O} the density of water kg/m^3
β the real water composite number of hydrate formation in the system, −
N_i the molar percentage of a certain component of natural gas, −
M_i the molar mass of a certain component of natural gas g/mol
T_C the equilibrium temperature K
T_0 the hydrate formation temperature K
P pressure Mpa
T_{Tem} temperature K
n_{NG} gas consumption mol
ΔP pressure drop Kpa
Q mass flow kg/h
T time min
φ hydrate volume fraction, −
α water cut, −
r gas consumption rate mol/min
μ apparent viscosity pa·s

REFERENCES

(1) Oignet, J.; Delahaye, A.; Torré, J.-P.; Dicharry, C.; Hoang, H. M.; Clain, P.; Osswald, V.; Youssef, Z.; Fournaison, L. Rheological study of CO_2 hydrate slurry in the presence of Sodium Dodecyl Sulfate in a secondary refrigeration loop. *Chem. Eng. Sci.* **2017**, *158*, 294−303.
(2) Sun, X.; Liu, D.-J. Progress in kinetic accelerator of carbon dioxide hydrate. *Chem. Ind. Eng. Prog.* **2018**, *37*, 517−524.
(3) Okwananke, A.; Hassanpouyouzband, A.; Farahani, M. V.; Yang, J.; Bukhanov, B. Methane recovery from gas hydrate-bearing sediments: An experimental study on the gas permeation characteristics under varying pressure. *J. Pet. Sci. Eng.* **2019**, *180*, 435.
(4) Sakurai, S.; Hoskin, B.; Choi, J.; Nonoue, T.; May, E. F.; Kumar, A.; Norris, B. W. E.; Aman, Z. M. Investigating hydrate formation rate and the viscosity of hydrate slurries in water-dominant flow: Flowloop experiments and modelling. *Fuel* **2021**, *292*, 120193.
(5) Hassanpouryouzband, A.; Joonaki, E.; Vasheghani Farahani, M.; Takeya, S.; Ruppel, C.; Yang, J.; English, N. J.; Schicks, J. M.; Edlmann, K.; Mehrabian, H.; Aman, Z. M.; Tohidi, B. Gas hydrates in sustainable chemistry. *Chem. Soc. Rev.* **2020**, *49*, 5225−5309.
(6) Ding, J.-X.; Liu, J.; Liang, D.-Q. Simulation of hydrate formation in submarine pipeline based on OLGA. *Oil Gas Storage Transp.* **2019**, *038*, 235−240.
(7) Gong, J.; Shi, B.-H.; Chen, Y.-C.; Song, S.-F. Submarine multiphase pipeline transport containing natural gas hydrate and its plugging risk prevention and control. *Nat. Gas Ind.* **2020**, *40*, 133−142.
(8) Liu, H.; Zhan, S.; Li, R.; Liu, Y.; Guo, P.; Wang, Z.; Du, J.; Wen, Y.; Dai, P.; Liao, H. High-efficiency natural-gas storage method involving formation of gas hydrate in water/oil-cyclopentane emulsion. *Chem. Eng. J.* **2020**, *400*, 125369.
(9) Liu, H.; Zhan, S.; Guo, P.; Fan, S.; Zhang, S. Understanding the characteristic of methane hydrate equilibrium in materials and its potential application. *Chem. Eng. J.* **2018**, *349*, 775−781.
(10) Ke, W.; Svartaas, T. M.; Chen, D. A review of gas hydrate nucleation theories and growth models. *J. Nat. Gas Sci. Eng.* **2019**, *61*, 169−196.
(11) Straume, E. O.; Morales, R. E. M.; Sum, A. K. Perspectives on Gas Hydrates Cold Flow Technology. *Energy Fuels* **2019**, *33*, 1−15.
(12) Sun, C.-Y.; Chen, G.-J. Study on the dynamics of hydrate formation in multiphase flow system by laser scattering method. *Chinese J. Popul. Resour. Environ.* **2003**, *13*, 25−29.
(13) Song, G.; Li, Y.; Wang, W.; Liu, S.; Wang, X.-Y.; Shi, Z.-Z.; Yao, S. Experimental investigation on the microprocess of hydrate particle agglomeration using a high-speed camera. *Fuel* **2019**, *237*, 475.
(14) Lv, X.-F.; Hu, S.-W.; Yu, D.; Tang, Y.-X.; Gong, J. Experimental study on hydrate formation characteristics based on FBRM. *Exp. Technol. Manag.* **2014**, *31*, 84−88.
(15) Lv, X.-F.; Wang, Y.; Li, W. Q.; Wang, L.-Y.; Ding, L.; Gao, F.; Gong, J. An experimental study of the hydrate blockage in the oil-dominated flow system. *Nat. Gas Ind.* **2014**, *34*, 108−114.
(16) Liu, H.; Guo, P.; Zhan, S.; Ma, P.; Wei, N.; Zhao, J.; Qiu, Y. Experimental investigation into formation/dissociation characteristics of methane hydrate in consolidated sediments with resistance measurement. *Fuel* **2018**, *234*, 985−995.
(17) Balakin, B. V.; Kosinska, A.; Kutsenko, K. V. Pressure drop in hydrate slurries: Rheology, granulometry and high water cut. *Chem. Eng. Sci.* **2018**, *190*, 77−85.
(18) Cao, X.; Yang, K.; Zhang, Y.; Yang, W.; Bian, J. Influences of particle micro behavior on gas-hydrate slurry flow pattern in pipeline. *J. Nat. Gas Sci. Eng.* **2021**, *93*, 104057.
(19) Ding, L.; Shi, B.; Lv, X.; Liu, Y.; Wu, H.; Wang, W.; Gong, J. Hydrate Formation and Plugging Mechanisms in Different Gas-Liquid Flow Patterns. *Ind. Eng. Chem. Res.* **2017**, *56*, 4173−4184.
(20) Liu, Z.; Vasheghani, F. M.; Yang, M.; Li, X.; Zhao, J.; Song, Y.; Yang, J. Hydrate slurry flow characteristics influenced by formation, agglomeration and deposition in a fully visual flow loop. *Fuel* **2020**, *277*, 118066.
(21) Sun, X.-Q. *Simulation of Multiphase Flow Field of Hydrate Slurry under High Pressure*; China University of Petroleum: Beijing, 2018.
(22) Shi, B.-H.; Yong, Y.; Liu, Y.; Li, M.-Z.; Ding, L.; Lv, X.-F.; Wu, H.-H.; Gong, J. Formation and flow characteristics of natural gas hydrate slurry in wax-containing and anti-polymer system. *Chem. Ind. Eng. Prog.* **2018**, *321*, 157−166.
(23) Jiang, K. *Study on Flow Plugging Mechanism of Gas Hydrate in Oil−Water System*; China University of Petroleum: East China, 2018.
(24) Yan, K.-L.; Sun, C.-Y.; Zou, B.; Jiang, S.-X.; He, J.; Tang, M. Inhibition performance of combined hydrate inhibitors in circulating pipelines. *Sci. Technol. Eng.* **2015**, *15*, 136−141.
(25) Dufour, A. F.; Herri, J. M. *Formation and Transportation of Methane Hydrate Slurries in a Flow Loop Reactor: Influence of a Dispersant, 4th International Conference on Gas Hydrates*, 2002.
(26) Li, Y.; Zhu, C.; Wang, W.-C.; Chen, Y.-L. Orthogonal experiment on influencing factors of stability of natural gas hydrate slurry. *Oil Gas Storage Transp.* **2011**, *30*, 685−689.
(27) Chen, J.; Chen, G.-J.; Yuan, Q.; Deng, B.; Tao, L.-M.; Li, C.-H.; Xiao, S.-X.; Jiang, J.-H.; Li, X.; Li, J.-Y. Insights into induction time and agglomeration of methane hydrate formation in diesel oil dominated dispersed systems. *Energy* **2019**, *170*, 604−610.
(28) Sun, C.-Y.; Chen, G.-J.; Yue, G.-L. The induction period of hydrate formation in a flow system. *Chin. J. Chem. Eng.* **2004**, *12*, 527−531.
(29) Chen, Y.; Shi, B.; Liu, Y.; Song, S.; Gong, J. Experimental and theoretical investigation of the interaction between hydrate formation and wax precipitation in water-in-oil emulsions. *Energy Fuels* **2018**, *32*, 9081−9092.
(30) Kashchiev, D.; Firoozabadi, A. Nucleation of gas hydrates. *J. Cryst. Growth* **2002**, *243*, 476−489.
(31) Zi, M.; Chen, D.; Wang, J.; Hu, P.; Wu, G.-Z. Kinetic and rheological study of methane hydrate formation in water-in-oil emulsion: Effects of emulsion composition and silica sands. *Fuel* **2019**, *255*, 115708.
(32) Wang, S.; Yang, M.; Liu, W.; Zhao, J.; Song, Y. Investigation on the induction time of methane hydrate formation in porous media under quiescent conditions. *J. Pet. Sci. Eng.* **2016**, *145*, 565−572.

https://doi.org/10.1021/acsomega.1c05127
ACS Omega 2022, 7, 599−616

(33) Wang, S.; Yang, M.; Li, K. Experimental analysis on the probability density distribution of methane hydrate induction times in porous media. *ChemistrySelect* **2018**, *3*, 3781−3786.
(34) Chen, Y.; Shi, B.; Lan, W.; Huang, F. Study on hydrate formation and dissociation in the presence of fine-Grain Sand. *Proceedings of the ASME Pressure Vessels and Piping Conference*; American Society of Mechanical Engineers, 2019.
(35) Song, G.; Li, Y.; Wang, W.; Jiang, K.; Shi, Z.; Yao, S. Hydrate formation in oil-water systems: Investigations of the influences of water cut and anti-agglomerant. *Chin. J. Chem. Eng.* **2020**, *28*, 369−377.
(36) Prah, B.; Yun, R. Pressure drop and flow characteristic of CO_2 hydrate slurry formation in the presence of anti-agglomerant in a flow loop facility. *J. Mech. Sci. Technol.* **2021**, *35*, 761−770.
(37) Basha, M.; Shaahid, S. M.; Al-Hems, M. L. Effect of water cut on pressure drop of oil (D130) -water flow in 4″Horizontal Pipe. *IOP Conf. Ser. Mater. Sci. Eng.* **2018**, *326*, 012002.
(38) Chen, Y.; Gong, J.; Shi, B.; Yao, H.; Liu, Y.; Fu, S.-K.; Song, S.-F.; Lv, X.-F.; Wu, H.-H.; Lou, X. Investigation into methane hydrate reformation in water-dominated bubbly flow. *Fuel* **2019**, *263*, 116691.
(39) Zhang, J.-B.; Wang, Z.-Y.; Liu, S.; Zhang, W.-G.; Yu, J.; Sun, B.-J. Prediction of hydrate deposition in pipelines to improve gas transportation efficiency and safety. *Appl. Energy* **2019**, *253*, 113521.
(40) Bai, D.; Chen, G.; Zhang, X.-R.; Sum, A. K.; Wang, W.-C. How Properties of Solid Surfaces Modulate the Nucleation of Gas Hydrate. *Sci. Rep.* **2015**, *5*, 12747.
(41) Darbouret, M.; Cournil, M.; Herri, J.-M. Rheological study of TBAB hydrate slurries as secondary two-phase refrigerants. *Int. J. Refrig.* **2005**, *28*, 663−671.
(42) Hashimoto, S.; Kawamura, K.; Ito, H.; Nobeoka, M.; Inoue, Y. Rheological Study on tetra-n-butyl Ammonium Salt Semi-Clathrate Hydrate Slurries. *7th International Conference on Gas Hydrates*; Hydrafact Ltd., 2011.
(43) Clain, P.; Delahaye, A.; Fournaison, L.; Mayoufi, N.; Dalmazzone, D.; Fürst, W. Rheological properties of tetra-n-butylphosphonium bromide hydrate slurry flow. *Chem. Eng. J.* **2012**, *193-194*, 112−122.
(44) Wang, W.; Fan, S.; Liang, D.; Li, Y. A model for estimating flow assurance of hydrate slurry in pipelines. *J. Nat. Gas Chem.* **2010**, *19*, 380−384.
(45) Jerbi, S.; Delahaye, A.; Oignet, J.; Fournaison, L.; Haberschill, P. Rheological properties of CO_2 hydrate slurry produced in a stirred tank reactor and a secondary refrigeration loop. *Int. J. Refrig.* **2013**, *36*, 1294−1301.
(46) Camargo, R.; Palermo, T. Rheological Properties of Hydrate Suspensions in Asphaltenic Crude Oil. *4th International Conference on Gas Hydrates*, 2002.
(47) Chen, G.-J.; Sun, C.-Y.; Ma, Q.-L. *Science and Technology of Gas Hydrates*, 2nd ed.; Chemical Industry Press, 2020.
(48) Bao, Z.-P.; Chen, G.-J.; Sun, C.-Y.; Dandekar, A.; Guo, S.-H.; Liu, B.; Mu, L.; Yang, L.-Y.; Li, W.-Z.; Chen, G.-J. Flow characteristics and morphology of hydrate slurry formed from (natural gas+diesel oil/condensate oil+ water) system containing anti-agglomerant. *Chem. Eng. Sci.* **2012**, *84*, 333−344.
(49) Shi, B.-H.; Chai, S.; Ding, L.; Chen, Y.-C.; Liu, Y.; Song, S.-F.; Yao, H.-Y.; Wu, H.-H.; Wang, W.; Gong, J. An investigation on gas hydrate formation and slurry viscosity in the presence of wax crystals. *AIChE J.* **2018**, *64*, 3502−3518.
(50) Song, G.; Li, Y.; Wang, W.; Jiang, K.; Ye, X.; Zhao, P. Investigation of hydrate plugging in natural gas+diesel oil+water systems using a high-pressure flow loop. *Chem. Eng. Sci.* **2017**, *158*, 480−489.
(51) Shi, B.; Ding, L.; Liu, Y.; Yang, J.; Song, S.; Wu, H.; Wang, W.; Gong, J. Hydrate slurry flow property in W/O emulsion systems. *RSC Adv.* **2018**, *8*, 11436−11445.
(52) Song, G.-C.; Li, Y.-X.; Wang, W.-C.; Liu, S.; Wang, X.-Y.; Shi, Z.-Z.; Yao, S.-P. Experimental investigation on the microprocess of hydrate particle agglomeration using a high-speed camera. *Chem. Eng. Oil Gas* **2017**, *46*, 38−43.
(53) Chen, G.-J.; Guo, T.-M. A new approach to gas hydrate modelling. *Chem. Eng. J.* **1998**, *71*, 145−151.
(54) Maeda, N.; Wells, D.; Hartley, P. G.; Kozielski, K. A. Statistical analysis of supercooling in fuel gas hydrate systems. *Energy Fuels* **2012**, *26*, 1820−1827.
(55) Wu, H.-H.; Yang, L.; Lv, X.-F. Experimental study on gas hydrate formation rate. *Exp. Technol. Manag.* **2014**, *31*, 36−40.
(56) Li, W.; Gong, J.; Lü, X.; Zhao, J.; Feng, Y.; Yu, D. A study of hydrate plug formation in a subsea natural gas pipeline using a novel high-pressure flow loop. *Pet. Sci.* **2013**, *10*, 97−105.
(57) Ding, L.; Shi, B.; Lv, X.; Liu, Y.; Wu, H.; Wang, W.; Gong, J. Investigation of natural gas hydrate slurry flow properties and flow patterns using a high pressure flow loop. *Chem. Eng. Sci.* **2016**, *146*, 199−206.
(58) Li, L.; Chen, X.-K.; Li, Q.-L. Effect of flow rate on formation process of CO_2 hydrate in high water cut system. *Petrochem. Ind.* **2019**, *48*, 52−57.
(59) Wang, H.-X.; Lian, Z.-H.; Wang, S.-L. Formation and influencing factors of gas hydrate in subsea pipeline based on OLGA. *Ocean Dev. Manag.* **2021**, *38*, 87−92.
(60) Turner, D. J. *Clathrate hydrate formation in water-in-oil dispersions*; Colorado School of Mine: Golden, CO, USA, 2005.
(61) Lv, X.-F.; Wang, Y.; Li, W.-Q.; Wang, L.-Y.; Ding, L.; Gao, F.; Gong, J. Experimental Study on slurry flow of natural gas oil hydrate. *Nat. Gas. Ind.* **2014**, *034*, 108−114.
(62) Talaghat, M. R. Prediction of induction time for natural gas components during gas hydrate formation in the presence of kinetic hydrate inhibitors in a flow mini-loop apparatus. *Can. J. Chem. Eng.* **2013**, *91*, 790−797.
(63) Talaghat, M. R. Experimental investigation of induction time for double gas hydrate formation in the simultaneous presence of the PVP and L-tyrosine as kinetic inhibitors in a mini flow loop apparatus. *J. Nat. Gas Sci. Eng.* **2014**, *19*, 215−220.
(64) Wang, S.-L.; Rao, Y.-C.; Zhou, S.-D.; Li, J.-M.; Wang, M. An experimental study on deep-water natural gas transmission based on the hydrate slurry flow technology. *Nat. Gas. Ind.* **2014**, *34*, 101−107.
(65) Lv, X.-F.; Shi, B.-H.; Wang, Y.; Tang, Y.-X.; Wang, L.-Y.; Gong, J. Experimental study on hydrate induction time of gas-saturated water-in-oil emulsion using a high-pressure flow loop. *Oil Gas Sci. Technol.* **2014**, *70*, 253−268.
(66) Moraveji, M. K.; Ghaffarkhah, A.; Sadeghi, A. Effect of three representative surfactants on methane hydrate formation rate and induction time. *Egypt. J. Pet.* **2017**, *26*, 331−339.
(67) Lan, W.-P.; Lin, D.-C.; Huang, F.-F.; Shi, B.-H.; Chen, Y.-C.; Wu, H.-H.; Gong, J. Experimental study on the formation and decomposition of methane hydrate in sand-containing stirred system. *Contemp. Chem. Ind.* **2020**, *49*, 1839−1846.
(68) Zhang, P.; Diao, Y.; Dong, Z.; Pei, S.; Wang, Q.; Ren, S.; Zhang, L. Effect of the surfactants on hydrate formation during methane storage process. *IOP Conf. Ser. Earth Environ. Sci.* **2020**, *605*, 012007.
(69) Wu, W.-Q.; Song, X.-M.; Wei, F.; Cai, H.-C. Effects of different surfactants on gas hydrate formation. *Oil Gas Storage Transp.* **2021**, *40*, 411−416.

https://doi.org/10.1021/acsomega.1c05127
ACS Omega 2022, 7, 599−616